

THESIS

THE EFFECT OF SINGLE, SHAPED SURFACE FLAWS ON DUCTILITY IN CAST ALUMINUM DOG
BONE SPECIMENS IN UNIAXIAL TENSION

Submitted by

Scott L. Wardwell

Department of Civil and Environmental Engineering

In partial fulfillment of the requirements

For the Degree of Master of Science

Colorado State University

Fort Collins, Colorado

Summer 2017

Master's Committee:

Advisor: Hussam Mahmoud

Rebecca Atadero
Scott Shuler

Copyright by Scott Lewis Wardwell 2017

All Rights Reserved

ABSTRACT

THE EFFECT OF SINGLE, SHAPED SURFACE FLAWS ON DUCTILITY IN CAST ALUMINUM DOG BONE SPECIMENS IN UNIAXIAL TENSION

Ductile fracture of structural, metallic alloys is of great interest to the engineering community. This interest has sparked many attempts in an effort to describe the fracture process for these ductile materials. The theory that stands out is that ductile fracture is driven by the process of void nucleation, growth and coalescence which, as the name suggests, allows voids to be created through nucleation, then follows their growth and coalescence until material failure occurs. In this process, a damage criterion is often selected and used to model and predict how ductile fracture will occur. While this modeling yields results with enough accuracy to be useable in practical applications, it relies on some initial idealized void geometry. These geometries are usually of cylindrical or spherical nature and do not capture the essence of the actual void geometry of real materials. Surface flaws, on the other hand, are often modeled to mimic their actual appearance in real materials. This being the case, little research has been conducted on actual void geometry or highly specific, three-dimensional surface flaw geometry. This study explores these relatively untouched regions of geometrical interest and their effect on the ductile fracture process through physical testing of specifically shaped surface flaws on structural grade aluminum. Additionally, aluminum demonstrates unique properties with respect to ductility. Other ductile materials often yield in tension then continue to stretch and withstand additional loading up to some maximum material strength then

stretch more until eventual failure. Many commercially available grades of aluminum however, fail almost immediately after reaching their maximum material strength. The results from this study are compared so that the effects of the specific shapes on ductility can be seen. The results suggest that, depending on the definition of ductility, it may be possible to easily increase material performance for ductile materials, which demonstrate the unique ductility profile seen in aluminum, by introducing specifically shaped surface flaws.

ACKNOWLEDGEMENTS

I would like to thank my advisor, Dr. Hussam Mahmoud, who has encouraged me to do my best in every step of my research. I am thankful for his insight and willingness to help me explore every idea, no matter how crazy, in order to reach the final goal. I would also like to thank my committee members, Dr. Rebecca Atadero and Dr. Scott Shuler, for supporting this research and my continued education.

Additionally, I would like to thank my lovely wife whose support and inspirational devotion continually encourage me to better myself and strive for perfection. To my family who has encouraged me through every endeavor I have taken. Thank you all for your love and support.

TABLE OF CONTENTS

ABSTRACT	ii
ACKNOWLEDGEMENTS	iv
CHAPTER 1.....	1
INTRODUCTION	1
1.1 Background	1
1.2 Objectives	3
1.3 Scope of Research.....	3
CHAPTER 2.....	5
LITERATURE REVIEW	5
2.1 Introduction	5
2.2 Description of Stress State	7
2.3 Void Growth	8
2.4 Lode Parameter.....	12
2.5 Void Coalescence	15
2.6 Void Spacing.....	18
2.7 Measurements of Ductile Fracture	20
2.8 Literature Review Summary.....	22
CHAPTER 3.....	25
PUBLICATION	25
3.1 Introduction	25
3.2 Test Setup	29
3.3 Testing.....	35
3.3.1 Control Specimen	35
3.3.2 Randomly Flawed Specimen	37
3.3.3 Spherically Flawed Specimen	42
3.3.4 Semi-Spherically Flawed Specimen	45
3.3.5 Cubically Flawed Specimen	48
3.4 Fractography	51

3.5 General Discussion.....	53
3.6 Secondary Cracking.....	59
3.7 Ductility Profile.....	61
3.8 Conclusion.....	62
CHAPTER 4.....	65
CONCLUSIONS & FUTURE WORK	65
WORKS CITED	69

CHAPTER 1

INTRODUCTION

1.1 Background

In fracture mechanics, material failure typically occurs in one of two ways: brittle and ductile fracture. Brittle fracture, which is the first and most recognizable form of fracture, is the most understood of these two mechanisms. The process of brittle fracture is marked by the sudden and complete fracture of a material with very little plastic deformation. This fracture pattern is often seen in materials at low temperatures and highly constrained conditions and has been thoroughly investigated.

The second mechanism of material failure in fracture mechanics is ductile fracture. Ductile fracture is often presented with large amounts of plastic deformation prior to failure. This process also presents itself with a cup and cone appearance of a materials fracture surface. The appearance of the fracture surface is thought to be caused by slow crack growth inside of the material being studied, which is in direct opposition to the incredible speed of crack growth in brittle fracture. Ductile fracture is apparent in many cases of real world material failure.

The evidence of ductile fracture occurrence, under large inelastic deformations, in real world materials makes this failure mode a topic of great interest to the engineering community. To that end, many studies have been conducted to explain and predict ductile fracture in structural materials. Through continued exploration into this fracture process the predominate theory of void nucleation, growth and coalescence was formed. This theory shows the

progression of fracture starting with the formation of voids within the material in question. These voids form and grow with the application of stress until they reach a point where they can coalesce and form a crack. This crack then propagates through continued void coalescence until material failure.

The idea of void nucleation, growth and coalescence is widely accepted and used in much of the research conducted on ductile fracture. Many variables have been tested with this idea in mind. The variables considered include void shape, void spacing, number of voids considered and crack tip interaction. Often the void shapes considered are idealized as cylindrical, spherical or ellipsoidal in nature. Voids observed in real materials however do not conform to the idealized shapes considered. These real voids often present with random shape and volume. Investigations into the real shapes of voids are not often conducted; therefore, little material is available on the matter.

Research in to the effect of specific, three-dimensional surface flaw shapes on ductile fracture is likewise sparse. Much of the research material available for this aspect assumes that if a surface flaw is present, it exists in the form of a crack. These cracks are modeled in a fashion consistent with cracks observed in real materials, which do not often have recognizable shape or three dimensional properties. This area of research is also relatively unexplored due to the fact that great measures are taken to ensure materials used for real world applications are free of any surface flaws.

This research project is aimed at addressing the previously mentioned areas of actual void shape and three-dimensional surface flaw shape effect on ductile fracture. This study

seeks to address the importance of these shapes on the fracture process through physical material testing. It also aims to explore the extent to which void shape and surface flaw shape may be linked.

1.2 Objectives

Research in the College of Civil and Environmental Engineering at Colorado State University was conducted to explore the effect of specifically shaped, three-dimensional surface flaws on the process of ductile fracture. Physical material testing was conducted to investigate the following:

- The effect of specifically shaped surface flaws on the ductile fracture process;
- The effect of randomly shaped surface flaws on the ductile fracture process;
- The effect of surface flaw volume on the ductile fracture process;
- The possible link between the behavior of internal material voids and the behavior of external surface flaws;
- The overall performance, with respect to overall ductility and maximum stress, for each flaw shape;

1.3 Scope of Research

To achieve the objectives discussed in Section 1.2, the scope of this research is limited in the following ways:

- Three unique and specific surface flaw geometries were utilized to assess the effect of flaw shape on the ductile fracture process;

- Randomly shaped surface flaw geometries were utilized to assess the effect of flaw shape on the ductile fracture process;
- A single consistent material was used in all testing;
- All test specimens were forged using an identical process;
- All tests were conducted in uniaxial tension under identical conditions;
- Material impurity from the forging process is ignored as it is assumed to be equally present in each test specimen making its effect equally present in all test specimens;
- All surface flaws were removed from the testing specimen except the flaw being tested;

CHAPTER 2

LITERATURE REVIEW

2.1 Introduction

In fracture mechanics, the fracture of structural materials is generally viewed as either ductile or brittle, although it is generally a combination of both. Due to this classification, existing analytical models are geared toward predicting fracture under fairly specific restrained conditions. While this idea makes different cases of fracture easier to categorize and analyze, doing so can often yield inaccurate predictions of fracture. In most cases, fracture has been observed to be at least partially brittle and partially ductile at some time during the same fracture process. This interaction of ductile and brittle fracture is not well understood and largely ignored. The interaction between these two fracture criteria, though important, is not studied in detail. This is because existing models of fracture prediction tend to give an accurate enough result negating the necessity to provide more detail. While this line of thought may not be very thorough, it works well for most practical applications.

Brittle fracture is the most accurately understood of the two fracture classifications. The defining features of brittle fracture include limited pre-crack strain and very limited plastic deformation. Brittle fracture often occurs as the result of several different variables. The most prominent of these tend to be the temperature and the constraint conditions of the material being analyzed. The colder the material is and the more constrained it is the more likely it is that the material will fracture in a brittle manner. This classification of fracture is uniquely suited for analysis by traditional fracture mechanics, which requires the assumption of the

presence of a crack and is based on the concept of energy release rate. When considerably large pre-crack plastic strain is observed or the absence of initial defects in the material are assumed, brittle fracture can no longer be used.

Ductile fracture allows for the assumption of no initial material defects and one of its defining features is very large pre-crack plastic deformation. In ductile fracture, a ductile material is introduced to stress through tensile, compressive or a complex combination of loadings. The material at some point will reach a state where plastic strain is achieved and will then begin to deform and stretch out. After some amount of plastic deformation, a crack will form near the center of the strained zone and continue to open towards the outer edges of the material. Once a significant portion of the material has been separated, the crack will quickly propagate through the rest of the material in a plane oriented approximately 45 degrees from the initial crack plane. This process leads to the classic cup and cone appearance of the material that has been associated with ductile fracture.

The physical evolution of ductile fracture is thought to be caused by the process of void nucleation, growth and coalescence. In this process, microscopic inclusions in the material matrix under tension allow for the separation of the inclusion and material in question. This separation causes microscopic voids to form or nucleate. Continued loading causes the voids to grow, usually along the grain boundaries of the material matrix. After significant growth, these voids begin to coalesce and form what is perceived as a crack. The coalescence of voids continues until the material is completely severed.

2.2 Description of Stress State

For most models of ductile fracture, a description of the stress state is necessary to adequately describe it. Consider an arbitrary Cauchy stress tensor $\boldsymbol{\sigma}$ with principle stresses denoted σ_1 , σ_2 and σ_3 such that $\sigma_1 \geq \sigma_2 \geq \sigma_3$. The three stress invariants of the stress tensor can be defined as

$$I_1 = \sigma_1 + \sigma_2 + \sigma_3 \quad (1)$$

$$J_2 = \frac{1}{2} \boldsymbol{\sigma} : \boldsymbol{\sigma} = \frac{1}{6} [(\sigma_1 - \sigma_2)^2 + (\sigma_2 - \sigma_3)^2 + (\sigma_3 - \sigma_1)^2] \quad (2)$$

$$J_3 = \frac{1}{3} \boldsymbol{S} \cdot \boldsymbol{S} : \boldsymbol{S} = \det(\boldsymbol{S}) = (\sigma_1 - \sigma_m)(\sigma_2 - \sigma_m)(\sigma_3 - \sigma_m) \quad (3)$$

Where \boldsymbol{S} is the deviatoric stress tensor and σ_m is the mean stress. Since the deviatoric stress is defined as $\boldsymbol{S} = \boldsymbol{\sigma} + p\boldsymbol{I}$, where p is the hydrostatic pressure and \boldsymbol{I} is the unit tensor, it can be seen that $S_1 \geq S_2 \geq S_3$. This allows for the mean stress, denoted σ_m , and the von Mises stress, denoted $\bar{\sigma}$, to be defined as functions of the invariants and written as

$$\sigma_m = \frac{I_1}{3} \text{ and } \bar{\sigma} = \sqrt{3J_2} \quad (4)$$

and the normalized third deviatoric stress invariant can be written as

$$\xi = \frac{27}{2} \frac{J_3}{\bar{\sigma}^3} = \frac{3\sqrt{3}}{2} \frac{J_3}{J_2^{3/2}} \quad (5)$$

where $-1 \leq \xi \leq 1$. Equation (5) then characterizes the relationship between the major and minor principle stresses, σ_1 and σ_3 , and the intermediate principle stress, σ_2 . The hydrostatic pressure (p), the stress triaxiality (η) and the Lode angle (θ) can then be expressed as

$$p = -\sigma_m = -\frac{1}{3}(\sigma_1 + \sigma_2 + \sigma_3) = -\frac{I_1}{3} \quad (6)$$

$$\eta = \frac{\sigma_m}{\bar{\sigma}} = -\frac{p}{\bar{\sigma}} = \frac{I_1}{3\bar{\sigma}} \quad (7)$$

$$\theta = \frac{1}{3} \arccos \xi \quad (8)$$

and the normalized Lode angle, or Lode angle parameter, can be written

$$\bar{\theta} = 1 - \frac{6\theta}{\pi} = 1 - \frac{2}{\pi} \arccos \xi \quad (9)$$

where $-1 \leq \bar{\theta} \leq 1$. From the studies by Wierzbicki and Xue (2005) and Bai and Wierzbicki (2008), it can be seen that $\bar{\theta} = 1$ corresponds to axisymmetric tension ($\eta = 1/3$) and equi-biaxial compression, $\bar{\theta} = 0$ corresponds to generalized shear ($\eta = 0$) and plastic strain ($\eta = \pm \sqrt{3}/3$), and $\bar{\theta} = -1$ corresponds to axisymmetric compression ($\eta = -1/3$) or equi-biaxial tension ($\eta = 2/3$).

2.3 Void Growth

Initial work on void growth was started by McClintock (1968) who studied the growth of long cylindrical voids in a non-hardening material, pulled in the direction of its axis while subject to transverse tensile stresses. With this research, McClintock started to find the relation between the growth of a void and imposed stress and strain. Also noticed was that the expansion of the void per unit of applied strain increases exponentially with transverse stress. Following this research, Rice and Tracey (1969) conducted similar analysis to determine the relationship between void growth and stress triaxiality for an isolated spherical void in a remotely uniform stress and strain rate field. The spherical void is thought to be more realistic as it mimics the shape usually observed in physical testing. This void was also assumed to be

set in an incompressible, rigid-perfectly plastic solid. Through their research, Rice and Tracey (1969) also confirmed the exponential trend between void growth and stress triaxiality. These two studies were the first to suggest that the fracture of ductile metal is dependent on stress triaxiality. Through these two studies the exponential function describing the effect of stress triaxiality on the damage evolution of ductile fracture, in terms of void growth rate, was created. This function is expressed

$$\frac{d \ln f}{d \bar{\epsilon}} = c_1 \exp(c_2 \eta) \quad (10)$$

where f is the porosity of the material in question and $\bar{\epsilon}$ is the equivalent plastic strain. Here c_1 and c_2 are material constants suggested to be 0.850 and 1.5 respectively in the original work of Rice and Tracey (1969).

The damage evolution model stated in equation (10) was later confirmed by Gurson (1977) and Tvergaard and Needleman (1984). They were able to improve upon this and create the Gurson-Tvergaard-Needleman model. This model is given as

$$\frac{d \ln f}{d \bar{\epsilon}} = 1.5 q_1 q_2 \sinh(1.5 q_2 \eta) \quad (11)$$

where q_1 and q_2 are constants that can be taken to be 1.5 and 1 as suggested by Tvergaard and Needleman (1984). It is worth mentioning that these models are tested predominately in the high stress triaxiality ranges and in those ranges equation (11) can be reduced to equation (10). These models also take the porosity of the material in question as the only microstructural variable and it is viewed as a damage indicator.

Several models have been proposed based on the physical evolution of ductile fracture. The most prominent of these models, and the model upon which many others are based, is the Gurson Model. Following the ideas put forth by McClintock (1968) and Rice and Tracy (1969), Gurson (1977) examined the effect of long cylindrical and spherical voids on the yield loci of ductile void-matrix aggregate. In this research, Gurson makes use of a “unit” cube made of porous material. This aggregate of voids and ductile matrix is idealized as a single void in a rigid-plastic cell where the void volume fraction of the cell is equal to that of the aggregate. The unit cells used by Gurson can be seen in Figure 1-1.

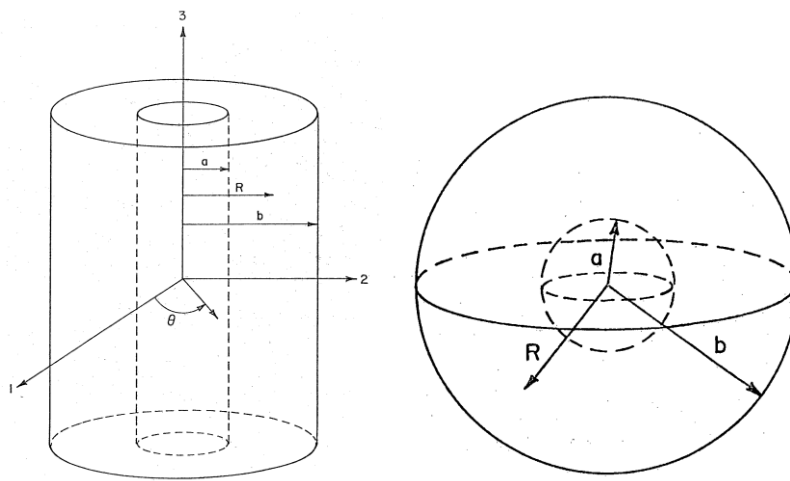


Figure 1-1: Depiction of Representative Unit Cells Used in Gurson's Research (Gurson 1977)

This “unit” cell is also presumed to behave as the aggregate would, allowing for void growth when yielding with a positive hydrostatic component of macroscopic stress. More conditions assumed on this void-matrix require it to be homogeneous, incompressible, rigidly-plastic, and a von Mises material. Through the use of the macroscopic rate of deformation, defined in terms of the velocity field on the surface of the unit cube, and several other complicated

relationships and conditions, Gurson (1977) was able to create one of the first approximate yield conditions for ductile fracture. This model was then modified by Tvergaard and Needleman (1984) and can be expressed in its most recognizable form as

$$\Phi = \frac{\sigma_e^2}{\sigma_m^2} + 2q_1 f^* \cosh\left(\frac{\text{tr}\sigma}{2\sigma_m}\right) - 1 - (q_1 f^*)^2 = 0 \quad (12)$$

where σ is the macroscopic stress tensor, σ_e is the equivalent von Mises stress, σ_m is the actual yield stress of the matrix material and f^* is the effective void volume fraction. f^* is taken to be

$$f^*(f) = \begin{cases} f & \text{if } f < f_c \\ f_c + \frac{1-f_c}{f_f-f_c}(f-f_c) & \text{if } f > f_c \end{cases} \quad (13)$$

where f is the void volume fraction, f_c is the critical void volume fraction at the onset of coalescence and f_f is the critical void volume fraction at final rupture.

Gologanu et al. (1993, 1994, and 1995) continued on the path set forth by the Gurson-Tvergaard-Needleman model and introduced the void shape change effect into the porosity evolution. Until this point the voids considered only grew in size, but not in shape. If a void was initially considered to be spherical or cylindrical, its growth was governed by the fact that it had to stay spherical or cylindrical. This allowed for the deviation of an initial void's size, but ensured it always remained the same shape. These idealized shapes work wonderfully for basic analysis, but fail to paint an accurate picture of real materials. Simple observation of real world ductile fracture cases suggests that actual materials have predominately non-spherical voids. The research conducted by Gologanu et al. (1993, 1994, and 1995) allowed for voids to become ellipsoidal and expand to become either oblate ellipsoids or prolate ellipsoids. This research led

to the proposal of the Gologanu-Leblond-Devaus model, which is viewed as a Gurson-like model.

2.4 Lode Parameter

The Gurson and Gurson-like models discussed are porosity based models and are only sensitive to stress triaxiality. This means that the equivalent plastic strain to fracture is only dependent on the ratio of the first invariant of the stress tensor and the second invariant of the deviatoric stress tensor shown by equation (7). In the moderate to high stress triaxiality ranges these models do well describing predominate tensile fracture, but fail when attempting to describe fracture in the low to negative stress triaxiality ranges. In these lower domains shear fracture is believed to dominate. The shear effect is often expressed in terms of Lode parameters or the third invariant of the deviatoric stress tensor. Experimental data collected by Xue and Wierzbicki (2008) and Kiran and Khandelwal (2014) have confirmed the importance of the shear effect in the formation and progression of fracture.

From a mechanistic perspective, the process of void nucleation, growth and coalescence is driven by two factors commonly referred to as void dilation and void shape/rotation. Under high triaxiality conditions spherically symmetric volume changes, or void dilation, is driven by hydrostatic stress. The components of that hydrostatic stress overwhelm the other shape-changing/rotation phenomenon caused by the deviatoric stress components and allow for exponential relationships to describe the void growth. The Rice-Tracey and Johnson-Cook criterion, which are identical under proportional loading and are expressed

$$\frac{d \ln f}{d \bar{\epsilon}} = c_1 \exp(c_2 \eta) \Rightarrow \bar{\epsilon}_f = c_1^{-1} \exp(-c_2 \eta) \Rightarrow \bar{\epsilon}_f = c_5 \exp(c_6 \eta) \quad (14)$$

where c_6 is assumed to be -1.5 and η is a transient parameter, is one example of this exponential relationship. In cases with moderate to low stress triaxiality, not much void dilation will be introduced. In these cases, the void shape-changing/rotation effects can no longer be ignored and stress triaxiality alone is no longer sufficient to predict the fracture locus of any ductile material being studied.

When moderate to low stress triaxiality cases are present the hydrostatic stress alone is no longer sufficient to describe the ductile fracture process. This is where the Lode parameter or Lode angle effect comes in. Though the Lode parameter effect is relatively unexplored, its importance in the ductile fracture process has been shown by Bao and Wierzbicki (2004), Wierzbicki et al. (2005), and Bai (2008) and confirmed by Barsoum and Feleskog (2007). Although the physical mechanisms behind the Lode parameter are not as clearly understood as those behind stress triaxiality, it is often thought to be associated with change in void shape or variation in void growth direction. While some studies, such as Xue (2008), consider the Lode parameter to exist intermittently, recent developments suggest it continually exists in all ductile fracture cases (Wen and Mahmoud, 2015a and 2015b).

Several models have been presented to show ductile fracture in the low stress triaxiality regions. Some of the more widely known and accepted models proposed include the maximum shear model and the Mohr-Coulomb fracture criterion (Bai and Wierzbicki, 2010). While both of these models do well to predict fracture in low triaxiality regions, the maximum shear stress fracture model has proven easier to use without the loss of accuracy. The normalized maximum shear damage criterion can be transformed into a function of $\bar{\theta}$ and expressed

$$\frac{\sigma_1 - \sigma_3}{\bar{\sigma}} = \cos\left(\frac{\pi}{6} \bar{\theta}\right) \quad (15)$$

It can be seen from equation (15) that the maximum shear criterion does not include any stress triaxiality-related parameters. With its main focus being on the Lode parameter, the maximum shear damage criterion does well at predicting ductile fracture in low stress triaxiality cases, but fails to predict fracture in high triaxiality zones. Similarly, the Gurson-like models discussed previously focus only on the stress triaxiality dependence of ductile fracture. This makes the Gurson-like models excellent predictors of ductile fracture in high triaxiality regions, but leads to their failure to predict fracture in low triaxiality regions.

Allowing the Lode parameter to continually exist suggests that it plays an important role in the ductile fracture process even in higher stress triaxiality cases. In high triaxiality ranges the Lode parameter plays a relatively small role as a damage modifier, while the hydrostatic stress's contribution is overwhelming. In negative triaxiality cases, where shear fracture prevails, the roles are reversed and the Lode parameter is responsible for the majority of the damage incurred. In medium to low triaxiality cases the two phenomena would compete and neglecting either of them can lead to an inaccurate estimate of damage. While the same could be said for the high and negative triaxiality cases, since one parameter generally overwhelms the other, several proposed models have been shown to predict fracture with reasonable enough accuracy.

With the importance of the Lode parameter and stress triaxiality on ductile fracture known, Wen and Mahmoud (2015a) proposed a damage model that incorporated both. This model, expressed

$$\bar{\epsilon}_f = c_7 \exp(c_8 \eta) \left[\cos\left(\frac{\pi}{6} \bar{\theta}\right) \right]^{c_9} \quad (16)$$

where c_7 , c_8 and c_9 are material constants, allows for good predictions of ductile fracture in all triaxiality ranges. It is worth mentioning that this model must be calibrated for each material it is used for since variations in materials are captured by the variation of the constants in the equation.

2.5 Void Coalescence

Macroscopic fracture toughness and the microstructure of the material can be linked through the use of micromechanical analysis of the fracture process. In the literature two types of mechanism-based approaches have been proposed. The Gurson-like models are considered to be examples of the first approach, where voids are considered implicitly using a continuum damage material model. These models are attractive when simulating extensive crack growth since modeling of individual voids is avoided, but requires a precise constitutive model for characterizing the void-containing material behavior. The second approach allows for voids to be considered explicitly. This is usually accomplished by modeling each void using refined finite elements as can be seen in Figure 2-2. This allows the exact implementation of void growth behavior to be achieved. The main difficulties with this approach are that, due to computational limitations, only a limited number of voids can be included and, in order to establish crack advance, a failure criterion for the ligament between voids is required.

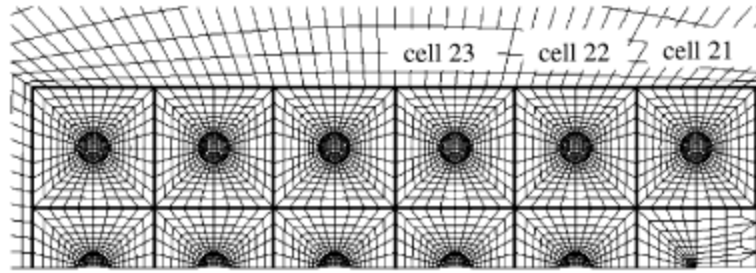


Figure 2-2: Example Finite Element Representation of Spherical Voids. (Gao et al. 2005)

Several theories have been proposed as to what criterion must be met in order for ligament failure to occur. Rice and Johnson (1969) proposed that coalescence of voids occurs when the size of the ligament between voids becomes equal to the vertical diameter of the void. Brown and Embury (1973) proposed that a slip plane can be drawn between voids and localized plastic flow causes ligament failure when the spacing between voids becomes equal to their length. Koplik and Needleman (1988) also suggested a method of determining the onset of void coalescence through unit cell analysis. The methods suggested here seem to be some of the more dominant methods used, but it is unclear as to which, if any, demonstrate a distinct advantage over the others.

Void coalescence is thought to occur through two different mechanisms: the void by void growth mechanism and the multiple void interaction mechanism. In the void by void growth mechanism, a crack forms between two adjacent voids and continues to open by ligament failure of adjacent voids. In this way, it proceeds void by void until failure occurs. A visualization of this process for a single row of spherical voids can be seen in Figure 2-3.

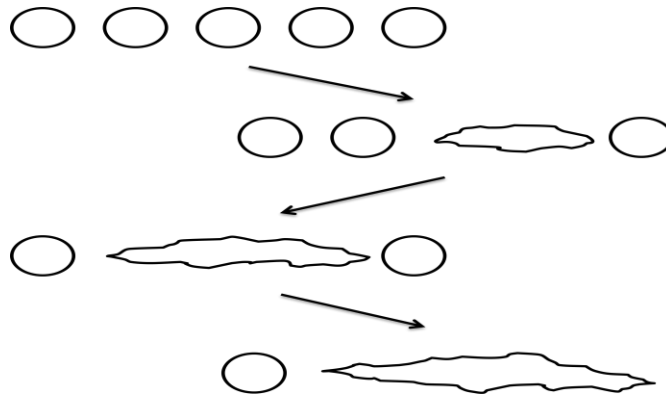


Figure 2-3. Depiction of Crack Growth in a Single Row of Spherical Voids Advancing Void by Void

In the multiple void interaction mechanism, several voids interact with each other both during crack initiation and subsequent crack growth. This would allow for several internal cracks to open up at the same time, presumably in or very near the same fracture plane as depicted in Figure 2-4.

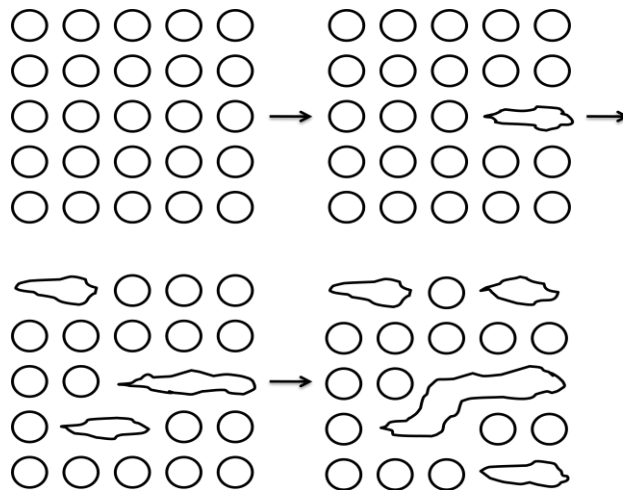


Figure 2-4: Multiple Void Interaction Depiction for Multiple Rows of Spherical Voids

Tvergaard and Hutchinson (2002) investigated these two distinct mechanisms and found that the occurrence of one or the other is primarily governed by the initial void volume fraction. For

materials with smaller initial void volume fractions, crack growth follows a void by void mechanism. Similarly, crack growth in materials with larger initial void volume fractions tends to follow a multiple void interaction mechanism.

The shape of the voids being considered plays a major role in the coalescence process. Most studies assume that voids are either cylindrical or spherical and other shapes are not greatly considered. Hom and Mcmeeking (1989) studied the interaction of these two void shapes on a crack tip. They were able to demonstrate that initially spherical voids tend to grow slower than initially cylindrical voids. They also suggest that the void grows faster towards a crack tip than away from it, showing a strong interaction between growing voids and the crack tip.

2.6 Void Spacing

The effect of void spacing in a ductile material being tested also plays a significant role in its fracture process. In real world applications, it is nearly impossible to manufacture materials with known defect size, shape and distribution. Often these defects, or inclusions, cluster in random locations causing random defect size and non-uniform distribution. While this is to be expected, most models assume a specific size, shape and uniform distribution for these inclusions in order to make reasonable calculations. This fact leads to a certain amount of inaccuracy when using any model to predict ductile fracture.

Several studies have been conducted to determine the effect void spacing has on the fracture process. In almost all cases it is assumed that a crack and voids are initially present.

Early work on the subject is focused on the interaction of a single void and the crack tip as depicted in Figure 2-5.

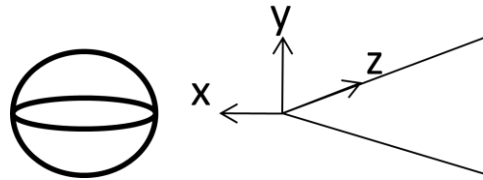


Figure 2-5: Example of a Single Void in Front of a Crack Tip

Aravas and McMeeking (1985) examined the interaction between the crack tip and a single cylindrical void under plain strain small scale yielding conditions. Hom and McMeeking (1989) studied the interaction of a single spherical void and the crack tip. Arun and Narasimhan (1999) investigated the effect of crack tip constraint on a single void's growth under mixed modes I and II loading. Multiple void interaction was later studied by Gu (2000) who considered a row of six cylindrical voids ahead of a plain strain, small scale yielding crack tip. Kim et al. (2003) considered a row of spherical voids ahead of a crack tip and confirmed Tvergaard and Hutchinson's result that the transition from the multiple void interaction mechanism to the void by void growth mechanism was controlled by the initial void volume fraction. They were also able to present a procedure to predict fracture initiation and growth.

Following these studies, Gao et al. (2005) investigated the effect of multiple spherical, prolate and oblate voids on the crack tip. They studied the effect of relative void spacing, void pattern and void shape for single and multiple rows of voids ahead of the crack tip as depicted in Figure 2-6.

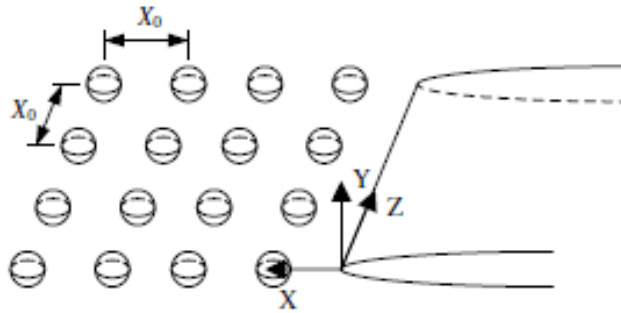


Figure 2-6 Multiple Rows of Voids Ahead of a Crack Tip (Goa et al. 2005)

Through this study, they were able to confirm the two void growth mechanisms put forth by Tvergaard and Hutchinson (2002). They were also able to show that the initial void volume fraction is not the only contribution that is being utilized in the void growth mechanism. For large initial void volume fractions, voids deviated from the crack growth plane and reduce the interaction among voids on the crack growth plane and delay the transition from void by void growth mechanism to the multiple void interaction mechanism. Increasing the relative void spacing intensifies the interaction among neighboring voids and facilitates the same transition of growth mechanisms (Gao et al., 2005). They were also able to show that oblate voids grew faster than spherical voids, and spherical voids grew faster than prolate voids when the oblate and prolate voids were positioned so that their long axis were parallel and perpendicular to the crack tip opening direction respectively.

2.7 Measurements of Ductile Fracture

The ductility of a material is often measured as the area under the line of its stress versus strain curve. To obtain this stress-strain curve, a sample of the material is taken and subjected to some force. The stress and strain values for this sample are then measured, as

continuously as possible, and their pairings are plotted. The discrete points of this plot are then connected with a smooth line and the stress-strain curve is obtained as illustrated in Figure 2-7.

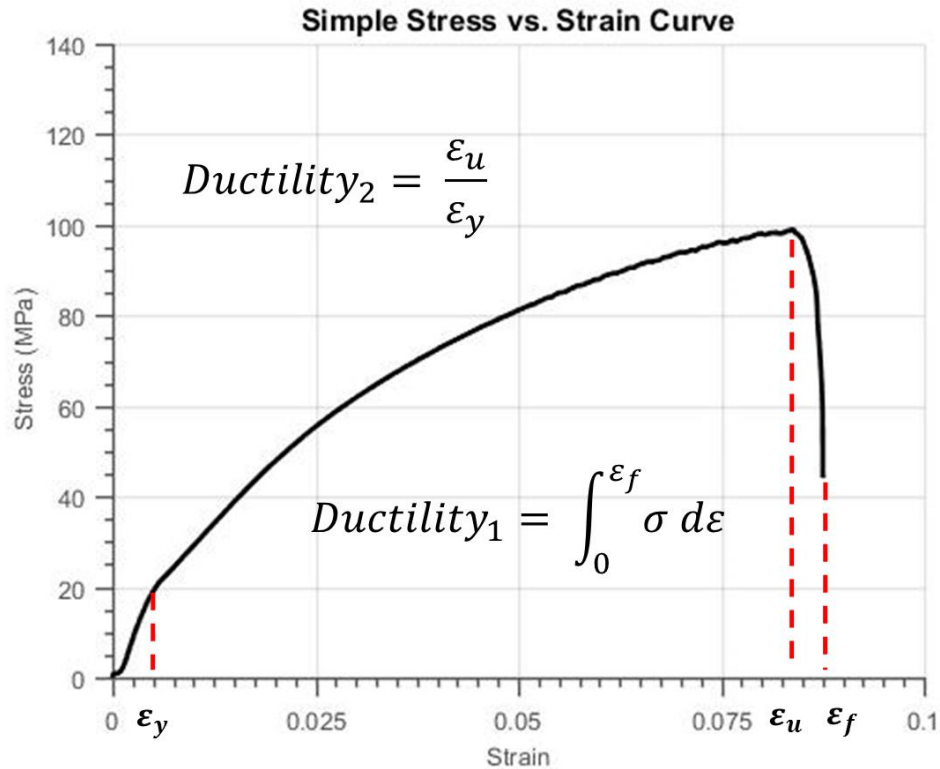


Figure 2-7: Stress-Strain Curve Example

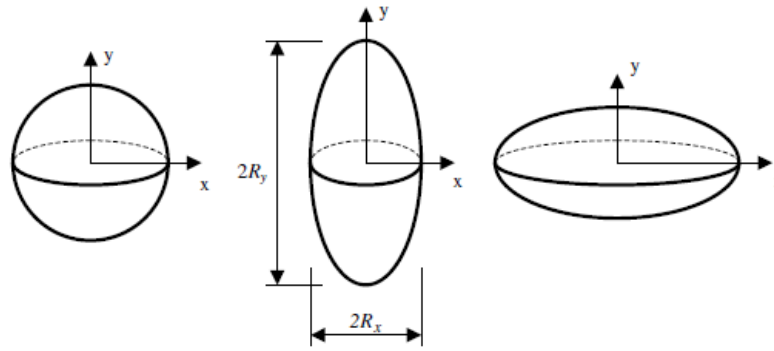
Since a ductile material by definition has large plastic deformation before failure, it is easy to compare a material’s ductility with that of another through this curve. The ductility of a material can also be defined as the maximum strain value (ϵ_u) divided by the yield strain (ϵ_y) obtained during testing, which can also be seen in this curve. Failure of a material is also seen in the stress-strain curve and is depicted as a sharp drop in stress with little to no additional strain recorded. While other information can be obtained through the use of these curves, these are the main factors of interest for this study.

It should be mentioned that these curves can be obtained for a variety of different loading cases. Here, cases of tension are of particular interest since most ductile fracture research is conducted with specimens in uniaxial tension. This trend can be seen in the work of McClintock (1968), Gurson (1977), Wen and Mahmoud (2015a), Spannaus (2016) and many others. Of course, cases of compressive loading can be studied, but a material's ductility is of little interest in this loading case.

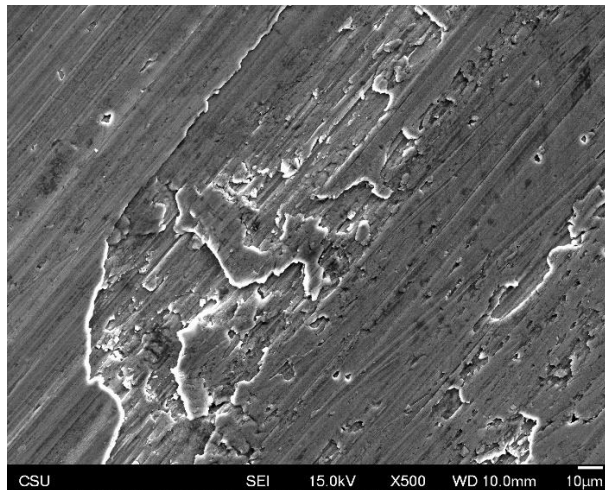
2.8 Literature Review Summary

The research that has been conducted on ductile fracture has considered many aspects that can affect the fracture process. Gurson (1977) studied the effect of cylindrical and spherical voids on ductile fracture and created one of the first ductile fracture models. Bao and Wierzbicki (2004) and many others were able to show the importance of the Lode parameter in ductile fracture and Wen and Mahmoud (2015a) were able to incorporate the Lode parameter into a viable ductile fracture model. The study by Gao et al. (2005) was able to show the effect of void spacing, multiple rows of voids and void orientation on crack tip propagation. However, in almost all of the research conducted, the effect of actual void and crack geometry is rarely taken into consideration.

A vast majority of studies conducted idealize the void inside of a ductile material as cylindrical, spherical or ellipsoidal. While this may make it easier to conduct calculations, it is not a true representation of voids in real world materials. The voids seen in actual materials are often randomly shaped and have jagged edges. This difference in idealized and real voids is easily seen in Figure 2-8.



(a)



(b)

Figure 2-8: (a) Idealized Void Shapes (Goa et al. 2005) (b) Aluminum With Random Void Shapes

When considering void growth, the idealized voids stay in the same shape that they were originally conceptualized as. That is to say, cylindrical voids stay cylindrical and spherical voids stay spherical. Even ellipsoidal voids that undergo “shape” change often only change by elongation of the ellipsoid in one direction at a time, much like in the study conducted by Gao et al. (2005). In real materials, voids grow by opening along grain boundaries within the material matrix, literally changing from one shape to another continuously throughout the

fracture process. A study conducted by Spannaus (2016) sought to address this problem slightly. In the study, tensile test specimens were made of cast steel and flaws of random shape and volume were injected into the cross-section. This study focused more on the flaw volume and it was found that, even for flaws that took up very small percentages of the cross-sectional area, ductility fell dramatically.

A similar approach has been taken when studying the effect of surface flaws on ductile fracture. Although this topic seems relatively unexplored, at least in three dimensions, the studies that have been published assume a flat crack that follows a straight line, a thumbnail crack, a through thickness crack or simply assume the crack has a blunt crack tip. A notable study conducted by Liu et al. (2015) explored the effect of a flaw of unique shape and angle on the fracture process. However, this study was conducted under uniaxial compression and unfortunately does not translate well into uniaxial tension which is the focus of the current study.

For both surface flaws and internal material voids, the issue of geometry effect on ductile fracture can be explored. This study seeks to explore those issues through physical material testing.

CHAPTER 3

PUBLICATION

3.1 Introduction

Fracture of structural materials is generally classified as brittle or ductile. In brittle fracture cases, limited pre-crack plastic strain, highly constrained crack tip and limited plastic deformation are assumed. Ductile fracture exhibits large plastic deformation and leads to a cup and cone appearance of the fracture surface. While both of these fracture classes have been studied extensively, simulating these processes still poses considerable challenges.

Ductile fracture of structural materials is a result of void nucleation, growth and coalescence. Numerous physical-based models have been proposed to mimic this behavior. Argon et al. (1975), Gurson (1977), Chu and Needleman (1980), Beremin (1981), Lee and Mear (1999), Benzerga and Leblond (2010) investigated and modeled the nucleation of voids. McClintock (1968), Rice and Tracey (1969), Gurson (1977) and Tvergaard and Needleman (1984) studied and contributed the foremost framework on void growth. The main findings on void coalescence were introduced by Thomason (1968) and Tvergaard and Needleman (1984). From these contributions, the physical-based Gurson-Tvergaard-Needleman (GTN) model was created. Gologanu et al. (1993, 1994 and 1995) also proposed the Gologanu-Leblond-Devaus (GLD) model. With both of these models, the porosity is usually the only microstructural variable and is utilized as a damage indicator. The GLD model also introduces the void shape change effect in to the porosity evolution. In these “Gurson-like” models, only sensitivity to stress triaxiality is present. This means that the equivalent plastic strain to fracture is only

dependent on the ratio of the first invariant of the stress tensor and the second invariant of the deviatoric stress tensor. While these models do well in predicting tensile fracture in moderate and high stress triaxiality domains, they generally fail to predict fracture in low and negative stress triaxiality domains. In these lower stress triaxiality domains, shear fracture is believed to dominate and is often expressed in terms of the Lode parameter or the third invariant of the deviatoric stress tensor.

Empirical ductile fracture models have also been developed in parallel with the physical-based models. Cockcroft and Latham, (1968), Brozzo et al. (1969), Oh et al. (1972), Oyane et al. (1980), Wilkins et al. (1980), Johnson and Cook (1985), Clift et al. (1990) and Ko et al. (2007) all performed extensive experimental programs on bulk materials and sheets to formulate these empirical models in the high stress triaxiality regions. Experiments in the low and negative stress triaxiality regions were comprehensively studied by Bao (2003), Bao and Wierzbicki (2004), Wierzbicki et al. (2005) and Bai (2008). The results from these tests and the analytical model developed by Bai and Wierzbicki (2010) all show that the Lode angle parameter as well as stress triaxiality play a major role in the successful prediction of strain and locus corresponding to ductile fracture. Recently, Wen and Mahmoud (2015a and 2015b) were able to incorporate both the stress triaxiality and Lode angle parameter in a unified model and successfully use it to predict ductile fracture of several materials in uniaxial tension.

In the literature, the prediction of fracture toughness is approached in two different ways. The first approach, using the Gurson-Tvergaard model, avoids detailed modeling of each individual void (Gurson, 1977; Tvergaard 1982). In this approach, voids are considered

implicitly and the model is favorably used in the simulation of extensive crack growth. The second approach explicitly considers individual voids and is modeled using refined finite elements. This approach allows for the exact implementation of void growth behavior where the first approach requires detailed modeling of the void-containing materials behavior during the ductile fracture process.

In the explicit approach, crack advancement is established through a failure criterion for the ligament between a void and the crack tip. Rice and Johnson (1969), Brown and Embury (1973) and Le Roy et al. (1981) all created different criteria for this void coalescence mechanism and Koplik and Needleman (1988) suggested a method to determine the onset of void coalescence by conducting unit cell analysis. While this approach allows for more exact calculation, only a limited number of voids can be modeled due to computational limitations. As a result, most of the published literature for this area is two-dimensional. Aravas and McMeeking (1985), Yan and Mai (1998) and Arun and Narasimhan (1999) all conducted studies to see the interaction effects between a single void and crack tip in the crack tip region. Using a row of cylindrical voids ahead of the crack tip, Tvergaard and Hutchinson (2002) investigated two distinct mechanisms for ductile crack initiation and growth, the multiple void interaction mechanism and the void by void growth mechanism. They found that these two mechanisms are governed by the initial void volume fraction. Lower initial void volume fractions lead to the void by void growth mechanism where only the void nearest the crack tip interacts with it and the crack progresses void by void. Higher initial void volume fractions lead the multiple void interaction mechanism where, as the name suggests, multiple voids ahead of the crack tip interact simultaneously during crack initiation and subsequent crack growth.

Further study into the effects of multiple void interaction was conducted by Gao et al. (2005) who studied single and multiple rows of spherical voids in front of a crack tip. The factors explored in this study included the effect of void spacing, void pattern and elliptical void shape on the fracture process. Through this work, the two mechanisms of void interaction suggested by Tveergaard and Hutchinson (2002) were confirmed. Another result of this work was noted in the effect of void spacing on crack growth. It was noted that the transition from the void by void growth mechanism to the multiple void interaction mechanism can be delayed by voids deviated from the crack plane. These deviated voids reduce the interaction of voids on the crack plane, slowing crack progression on that plane. Also of note was that increasing the relative void spacing intensifies the interaction of neighboring voids and facilitates the same mechanism transition.

Additionally, studies have been conducted on ductile aluminum alloys that illustrate the materials unique ductile nature through stress-strain curves. These curves demonstrate a definitive difference from curves of traditional ductile materials in that they quickly reach failure after reaching a maximum peak stress. Other ductile materials often exhibit some continued material performance and strain after the maximum stress value has been achieved. The stress-strain curves obtained in these studies are most often created from materials with no apparent flaws. This being the case, there is little information available on the effect of flaws on aluminums unique ductility “profile” as demonstrated through stress-strain curves.

While many studies have been conducted on the ductile fracture process, a vast majority of them idealize the shape of voids. These spherical and ellipsoidal shapes make

mathematical expression of the fracture process easier, but fail to capture the true nature of actual materials. In real materials, voids are present with random, often jagged, shapes and sizes. In a similar way, surface flaws or cracks in ductile materials are often idealized as two dimensional flat lines. This idealization is perhaps more understandable than that of void shape since most real world flaws present themselves in this manner. It is the intent of the current study to explore the possibility of more robust three-dimensional shapes of surface flaws on the ductile fracture process.

3.2 Test Setup

The first step in conducting this experiment was specimen fabrication. Although there are many commercially available grades of sheet aluminum with varying thicknesses and properties to choose from, it is inherently difficult to add specifically shaped flaws to pre-existing specimens. Sand casting, however, allows for very specific flaws to be added to the specimens with relative ease and for this reason was chosen as a viable fabrication method. To this end, a coal fire forge was constructed at the Engineering Research Center (ERC) at Colorado State University (CSU). This forge was fired and used to melt a single batch of recycled grade 6061 structural aluminum. This material was chosen for its known ductility, ease of fabrication and low melting point. The liquid metal was then poured into a sand cast mold and traditional dogbone specimens were forged in batches of three. Once at room temperature, these specimens were machined to the American Society for Testing Materials (ASTM) B557M Standard dimensions for cast aluminum alloys as depicted in Figure 3-1.

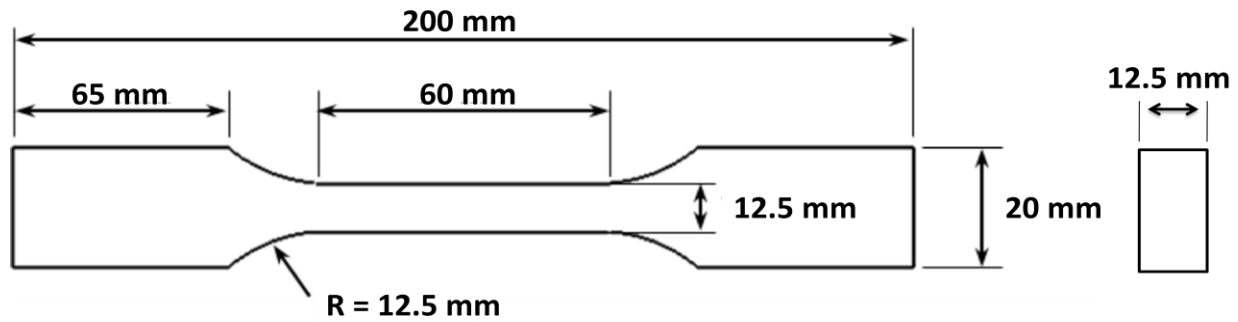


Figure 3-1: ASTM Standard Measurements for Cast Aluminum Specimen

All specimens were fabricated in the same manner and working conditions in order to minimize material variability. It should be mentioned that uncontrollable material variability is introduced in the form of gas bubbles, material impurity and foreign debris due to the casting process. The effect of these impurities will be examined later.

The material used in testing for this study was also analyzed using energy dispersal spectroscopy in a JSM-6500F field emission scanning electron microscope (SEM) located in the Imagine and Surface Science Laboratory (ISSL) at CSU. The results from this test reveal the chemical composition of the material that was tested for comparison to commercially available aluminum grades and can be seen in Figure 3-2. As can be seen in Figure 3-2, the material is composed of nearly 90% aluminum, 0.9% iron and 0.8% manganese and magnesium. These values very nearly match those given by The Aluminum Association for wrought aluminum and aluminum alloys. For 6061 designation aluminum, the limits for iron, manganese, and magnesium are given as 0.7%, 0.15% and 1.2% respectively. The carbon content for these materials are not listed so no comparison can be made, but the similarity in other elements

suggests the tested material will yield similar results to those that may be obtained if commercial grade material was used.

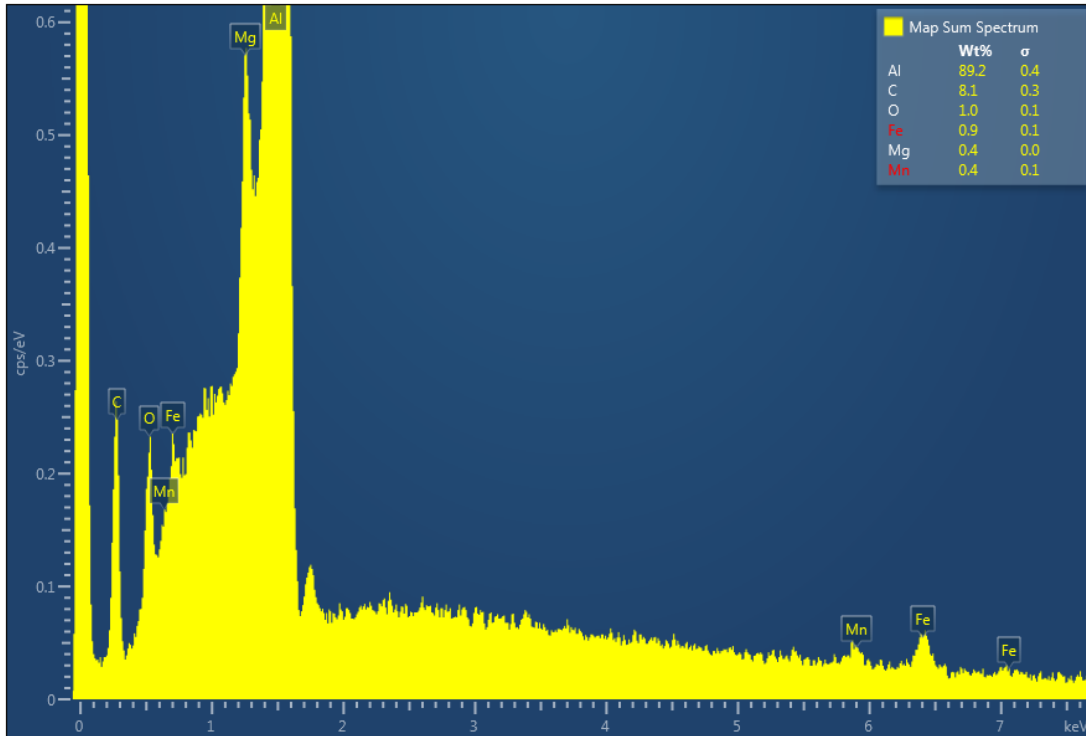


Figure 3-2: Chemical Analysis of Tested Material

A chemical mapping of the material used in testing was also obtained using the SEM and can be seen in Figure 3-3. The image at the top left depicts the material as seen through the SEM and the image at the top right is a layered map of all chemical elements within that image. The smaller images each represent the mapping of a single element within the testing material. As can be seen, the distribution of each element is fairly uniform throughout the image with only a few very small concentrations of non-aluminum elements. With the uniformity of material seen here, it can be assumed that material impurities introduced through the forging process discussed earlier will have a negligible impact on testing results.

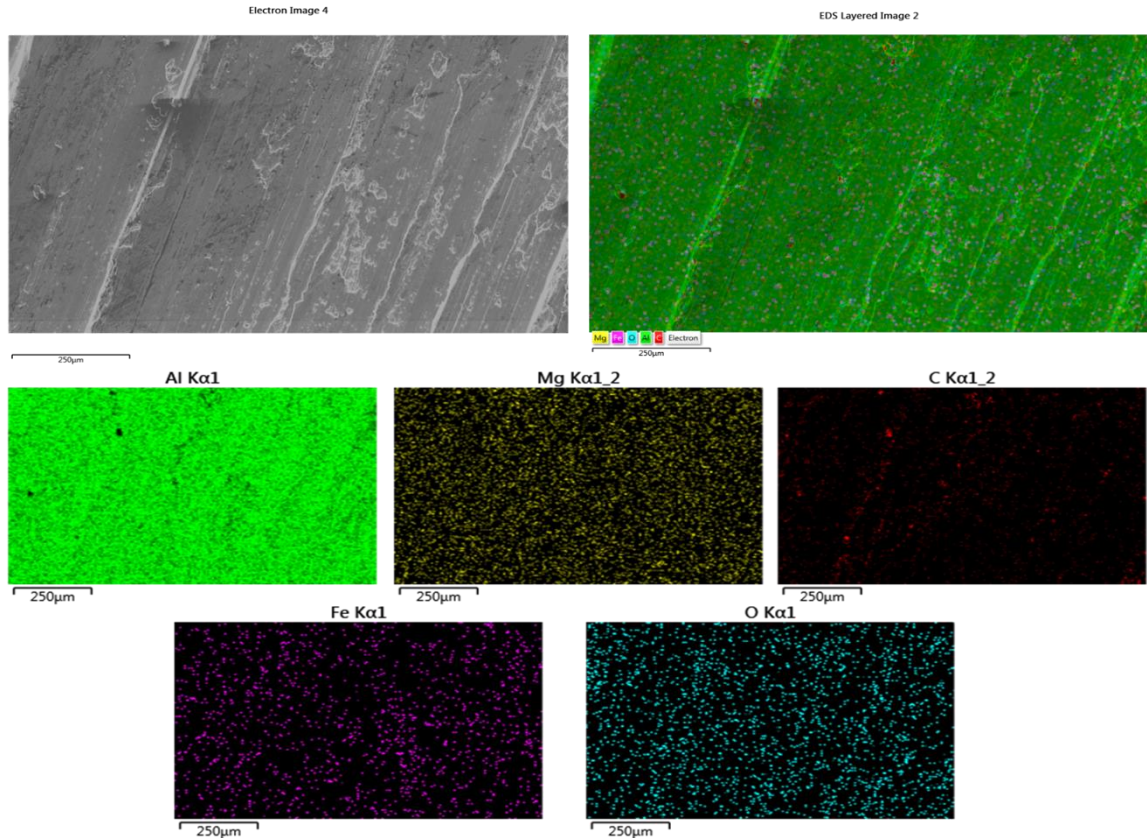


Figure 3-3: Chemical Element Distribution

An Instron model 4400R tensile testing machine with a 20 KN load cell located in the engineering lab at CSU was then utilized to test the forged and machined specimens in uniaxial tension. The specimens were tested at a rate of 2.5 mm/min and a temperature of 23 °C. The machine used was equipped with a built-in extensometer used to obtain the instant strain at every point during testing. The data collected was then utilized to create the entire stress-strain curve for each specimen tested.

For this experiment, four distinct flaw shapes were chosen. The first shape was chosen to be random with varying volume. This was accomplished by hand-shaping various amounts of aluminum around a spherical piece of glass. This shaped flaw was then inserted in the

specimen mold and the liquid aluminum was poured around it. Forming the specimen in this way allows for known surface flaws to be embedded in the specimen and ensures that there is minimal interaction between the flaw material and the specimen material. Each specimen created this way has a random flaw shape and flaw volume. The second shape tested was a spherical flaw embedded in the specimen in the same manner as the first. After machining, this flaw can be visualized as a hemispherical void in the side of the specimen. The third flaw tested was of semi-spherical shape and similarly embedded in the testing specimen with its long axis oriented parallel to the direction of force. This flaw can be imagined as the center third of the hemispherical void created by the spherical flaw. The final flaw shape was chosen to show what effect it may have when the edges are not as smooth as idealized shapes. To this end a cubically shaped flaw was embedded to achieve a pyramid shaped void in the specimen. For ease of use throughout this study, the specimens tested are named for the shape used in creation of the flaw and not the actual shape of the flaw being tested. Figure 3-4 depicts these four surface flaw shapes and their cross-sectional representations.

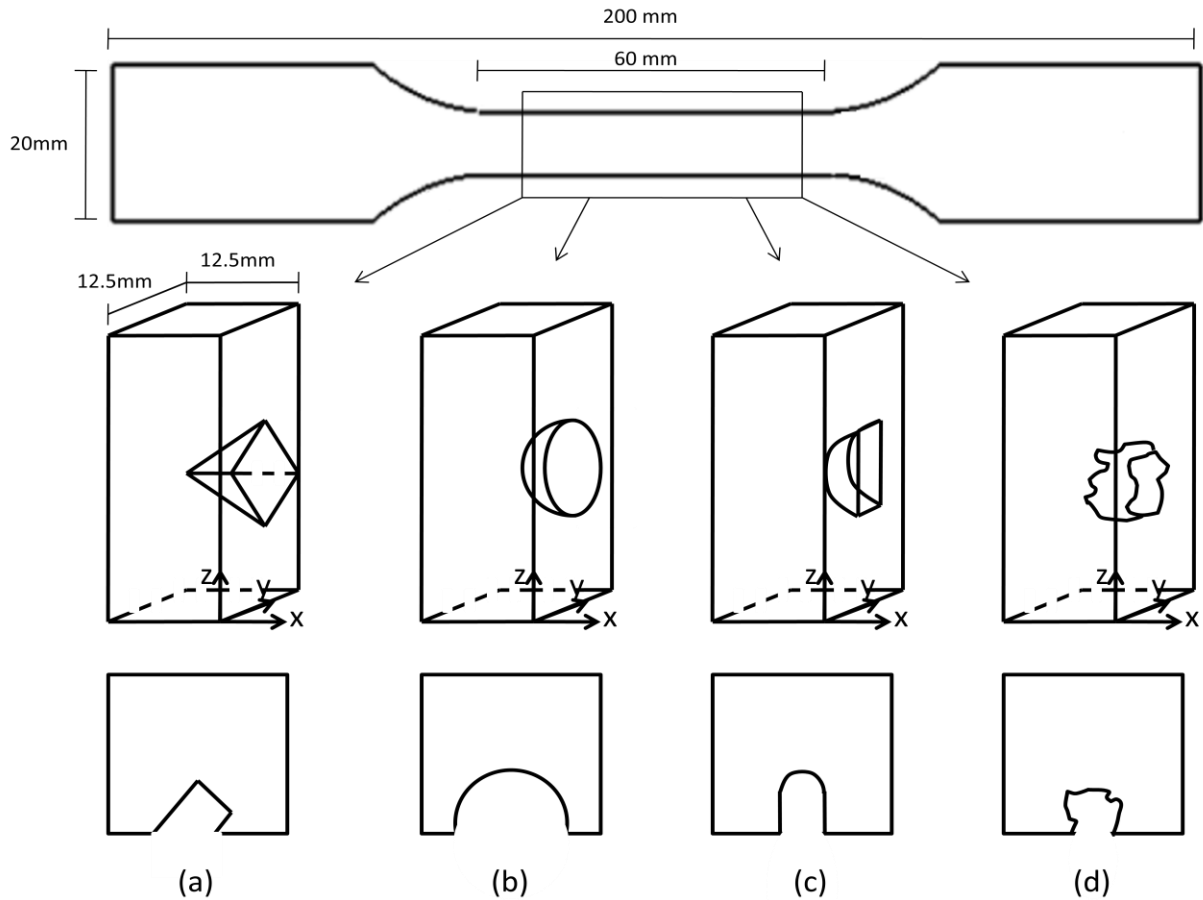


Figure 3-4: Representation of (a) Cubically Shaped Flaw (b) Spherically Shaped Flaw (c) Semi-Spherically Shaped Flaw (d) Randomly Shaped Flaw

Each of the final three voids was achieved through the use of shaped glass beads that were chosen because of their melting point and brittle nature. These two features allow the flaw shape to hold under the extreme temperatures encountered when pouring liquid aluminum and promote minimal interaction between specimen and flaw material. If by some chance the flaw material and aluminum became inseparable the low fracture stress of the glass in tension will ensure that it breaks long before the aluminum starts to fail.

3.3 Testing

3.3.1 Control specimen

The first set of specimens tested were control specimens with no apparent surface flaws present. These specimens were used to establish a baseline upon which other tests could be compared. Three control specimens were fabricated and tested to this end and the data collected is represented in Figure 3-5 as stress-strain curves.

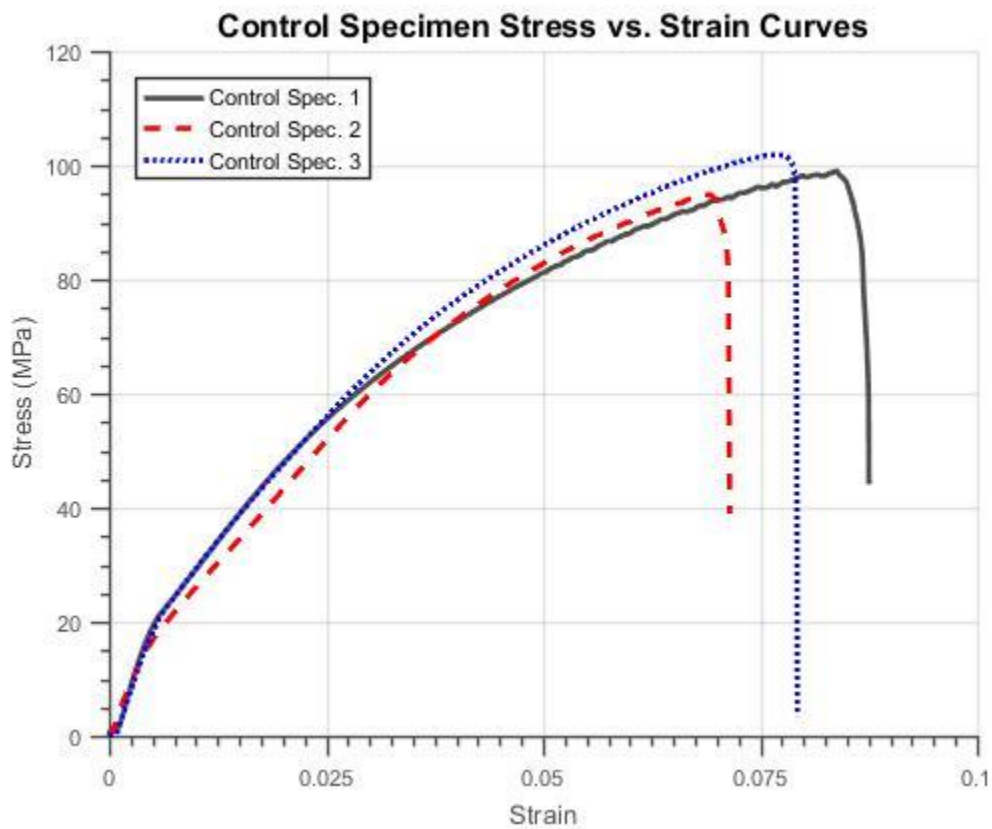


Figure 3-5: Stress-Strain Curves for Control Specimen

As can be seen in Figure 3-5, each specimen tested generated its own unique stress-strain curve. Each specimen, though forged in the same manner, exhibited slightly different measures of ductility. This is to be expected due to slight variation in the cross-sectional areas of each specimen's reduced section and the inherent randomness of material impurities introduced in the forging and casting process. The results show that control specimen one exhibited the most ductility and for the purpose of this study will be used as the baseline comparison. This specimen was chosen as a baseline because it is considered to be the most ductile of the three control specimens and does well to show the deviation of other tested specimen's ductility when compared side by side. These three specimens were also analyzed to obtain a standard deviation which will be applied to the testing of other flaw shapes to show theoretical material variability and obtain a clearer picture of the true effect of flaw shape on ductility.

The stress-strain curves obtained for these specimens are used as an indication of ductility. In addition to these curves, the physical specimen exhibited some evidence of the classic cup and cone fracture pattern often observed in ductile materials. This fracture pattern, pictured in Figure 3-6, serves as a secondary visual indication that the material behaves in a ductile manner as required for the current investigation.

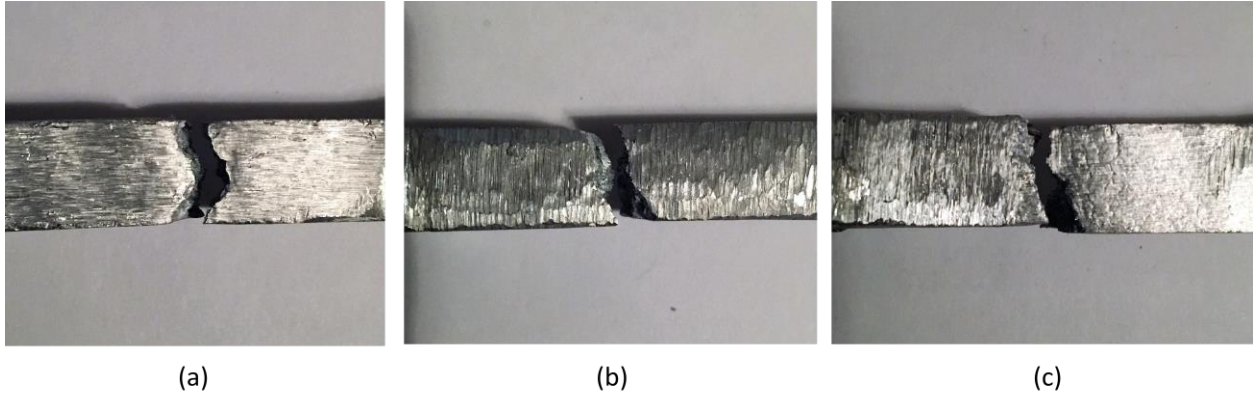
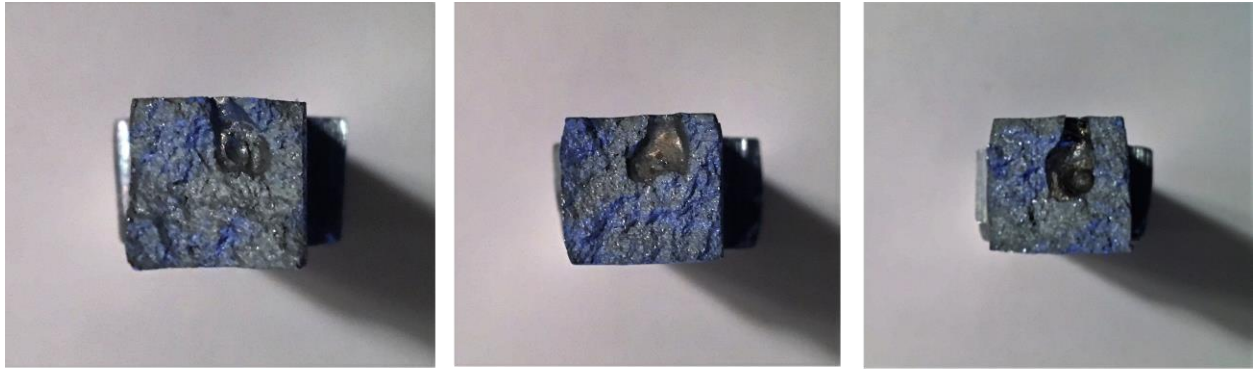


Figure 3-6: Cup-Cone Fracture Pattern Observed in (a) Control Specimen 1
(b) Control Specimen 2 (c) Semi-Spherical Specimen 3

3.3.2 Randomly Flawed Specimen

The next portion of testing was conducted on a total of eight specimens forged with randomly shaped flaws. While each batch of specimens was formed in groups of three, the ninth specimen exhibited signs of extreme malformation and was therefore excluded from testing. Each of these specimens were created with individually shaped flaws and flaw volume. Some examples can be seen in Figure 3-7.



(a)

(b)

(c)

Figure 3-7: Photos of Flaw Shape on Cross-Sectional Area of (a) Random Specimen 1
(b) Random Specimen 2 (c) Random Specimen 8

These flaws were chosen to represent the randomness of void shapes observed in real world materials. Although surface flaws and cracks do not generally present themselves in this manner, it is worth exploring as an extreme opposite to the smooth and ordered flaws examined later in this study. The results from these tests are shown in Figure 3-8 as stress-strain curves. Figure 3-8 shows the result of select random surface flaw specimens against control specimen one. These results were normalized with respect to cross-sectional area of the flaw to the cross-sectional area of the specimen. For the purpose of this test, the cross-sectional area of the flaw is measured at the flaws largest section. In this way, each specimen can be organized by the percentage of cross-sectional area removed by the surface flaw as noted in the legend of Figure 3-8. The results from these tests show a marked decrease in maximum strain with the presence of any surface flaw. They also suggest that as the surface flaws area percentage increases the maximum strain of the material decreases. This result conforms to expectations of material behavior as displayed in the research on cast steel put forth by Spannaus (2016). The ductility of all specimens in this category was also recorded and is displayed in Figure 3-9.

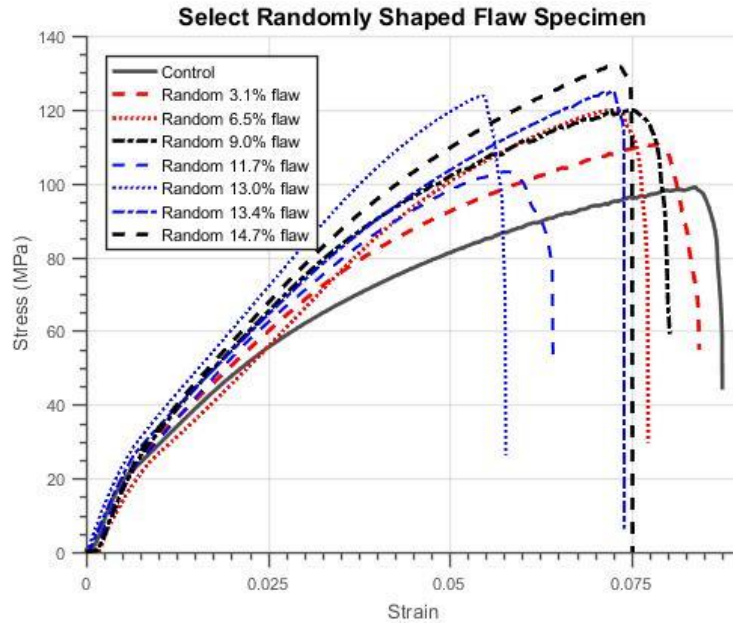


Figure 3-8: Randomly Shaped Flaw Stress-Strain Curves

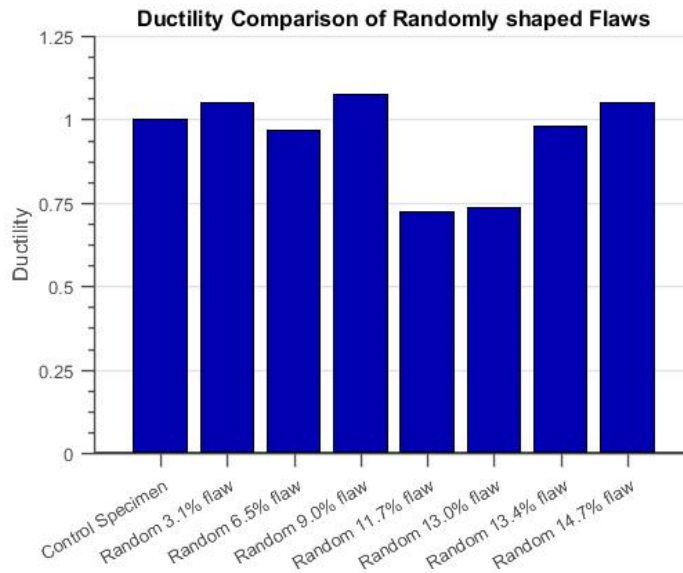


Figure 3-9: Ductility of Randomly Shaped Flaws

In order to compare the ductility of one specimen to another it was necessary to measure the area under each specimen's stress-strain curve then normalize by a constant,

which was chosen to be the ductility of control specimen one for the purposes of this study. In this way, a quantitative comparison can be made. In Figure 3-9 it can be seen that with the removal of increasing amounts of cross-sectional area from the specimen a general decrease in ductility is observed. While this general trend matches expectations, the specimens with 13.4% and 14.7% cross-sectional area removed appear perform as well or better than the control specimen. This observation is most likely due to the method by which ductility is measured. Because the maximum stress attainable increases by such a large amount for flawed specimen the area under the curve also increases by a large amount. For this reason, an additional measurement of ductility is calculated by dividing the maximum strain value obtained for each specimen by its yield strain value. The results from this calculation are shown in Figure 3-10 along with the potential variability in ductility as calculated from the control specimen group.

The results depicted in Figure 3-10 further demonstrate the general trend of decreasing ductility with increasing amounts of cross sectional area removed from the material. While the 13.4% and 14.7% flaws still demonstrate a curious increase in ductility over some of the flaws that remove smaller amounts of cross sectional area, they perform as traditionally expected overall. This small deviation from expectations can most likely be attributed to material variability, mistaken data accusation or analysis.

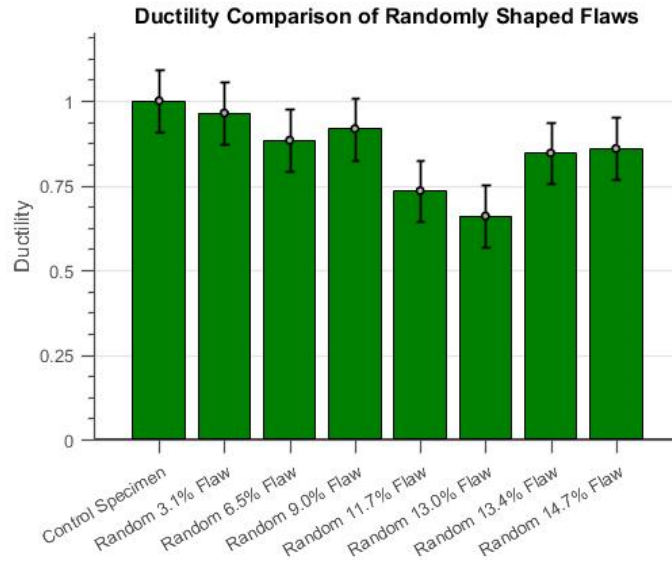


Figure 3-10: Additional Measurement of Ductility of Randomly Shaped Flaws

In Spannaus' research, circular uniaxial tension specimens were created with internal flaws of random shape and volume and tested in a similar manner as is presented in the current work. The results recorded by Spannaus' tests show a similar decrease in ductility with increase of flaw cross-sectional area. The difference between the two tests being discussed is that the previous research was conducted on internal flaws and the current study focuses on external flaws. With the apparent similarity in results expressed, it may be possible to link the behavior of macroscopic internal flaws to that of external flaws through a single unifying mechanism. Unfortunately, the results from this set of specimens are not plentiful enough to accurately attempt this link.

It can also be seen in Figure 3-8 that the random surface flaw specimens exhibit a higher maximum stress than is seen in the control specimen. This is also to be expected since adding a surface flaw increases stress triaxiality, which in turn increases the maximum stress attainable

by the flawed specimen. This result can be seen in a multitude of previous research efforts and is well documented.

3.3.3 Spherically Flawed Specimen

The next phase of testing was conducted on a set of three specimens that were forged with spherically shaped surface flaws. The shape for this specimen was chosen based on the idealized shapes for voids often tested in ductile fracture research. While the shape of voids within the material and the shape of surface flaws are often treated as completely different entities, it is believed that this shape may hinder the onset of fracture much like it can when considered in the void growth and coalescence process. Through this line of reasoning, it is expected that these specimens will perform better than the randomly shaped flaw specimens and worse than the control specimens. The primary data collected for these specimens was normalized in the same manner as previous specimens and the results are shown in Figure 3-11. These results show an overall increase in maximum strain over the control specimen. This is surprising given that the randomly shaped flaws exhibited decreased maximum strain when tested in the same manner. It would seem logical that these specimens would exhibit a similar decrease in maximum strain since they have a similar removal of cross-sectional area.

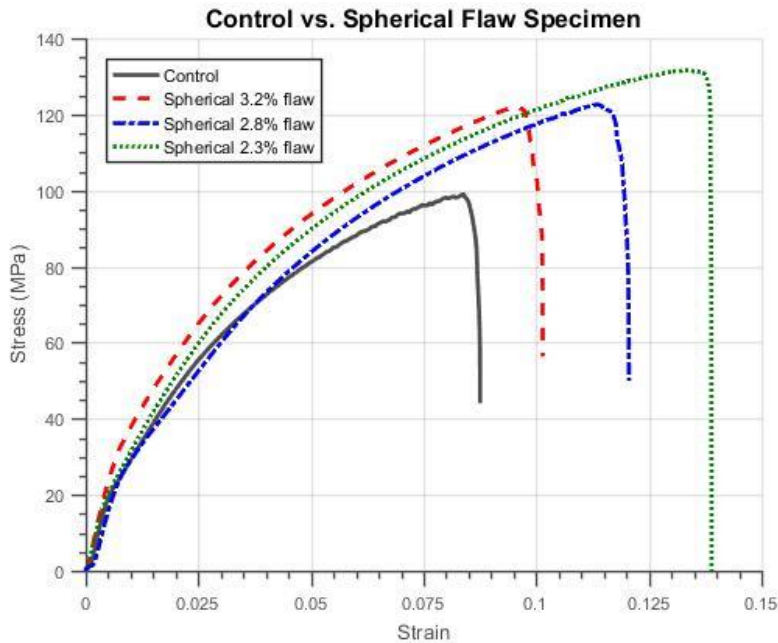


Figure 3-11: Spherically Shaped Flaw Stress-Strain Curves

The contradictory results shown in Figure 3-11 would suggest that the shape of the flaw plays a major role in the maximum achievable strain of each specimen since this is the only variable that has changed. The ductility of these specimens was also measured and is shown in Figure 3-12. The results for these spherically shaped surface flaws show a definitive increase in ductility over the flawless control specimen. This is most notable for the specimen with 2.3% of the cross-sectional area removed which had a measured ductility of over two times that of the control specimen. Improvement is seen even with up to 3.2% of the specimen's cross-sectional area removed by the flaw with an increase in ductility of approximately 50%.

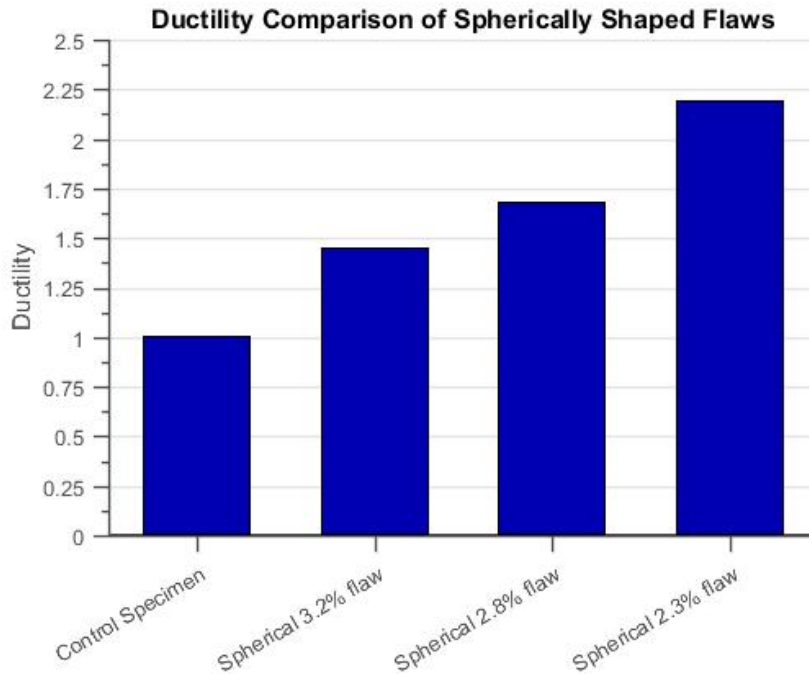


Figure 3-12: Ductility of Specimens with Spherically Shaped Flaws

As with the control specimens, an additional measurement of ductility is calculated using the maximum and yield strain values for each specimen and is depicted in Figure 3-13. The results shown in this figure further demonstrate the noticeable increase in ductility for specimens with flaws of a spherical shape. It can be seen that the ductility for the specimen with 2.3 % of the cross-sectional area removed is increased by nearly 60% percent over that of the control specimen.

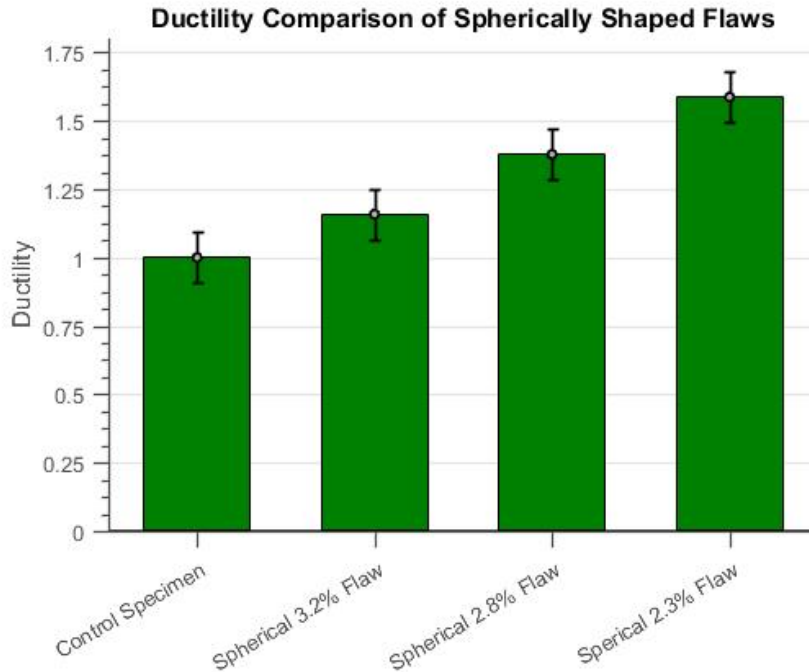


Figure 3-13: Additional Measurement of Ductility of Spherically Shaped Flaws

This result is surprising given testing on the randomly shaped surface flaws showed generally decreased ductility with any amount of cross-sectional area removed from the total area due to surface flaws. This result also shows that the shape of the surface flaw does indeed impact the overall performance of the material but in an opposite direction than as expected. In most studies of fracture, the mere presence of a surface flaw or crack negatively impacts material performance. Here however, the spherical surface flaws appear to enhance material performance.

3.3.4 Semi-Spherically Flawed Specimen

The next phase of testing was conducted on three specimens with semi-spherical shaped surface flaws. The shape for surface flaws in these specimens was chosen because of its

similarity to the previously tested spherically flawed specimens. Here the outer two thirds of the sphere are removed and the effect of straight edges may be tested while the crack tip presented remains very nearly the same. The data collected was again normalized as previously discussed and is shown in Figure 3-14. Similar to the results obtained for the spherically flawed specimens, the specimens with semi-spherically shaped flaws display an increased maximum strain. The results depicted in Figure 3-14 again suggest the importance of flaw shape on the ductile fracture process, since the only variable changed for this stage of testing was the flaw shape.

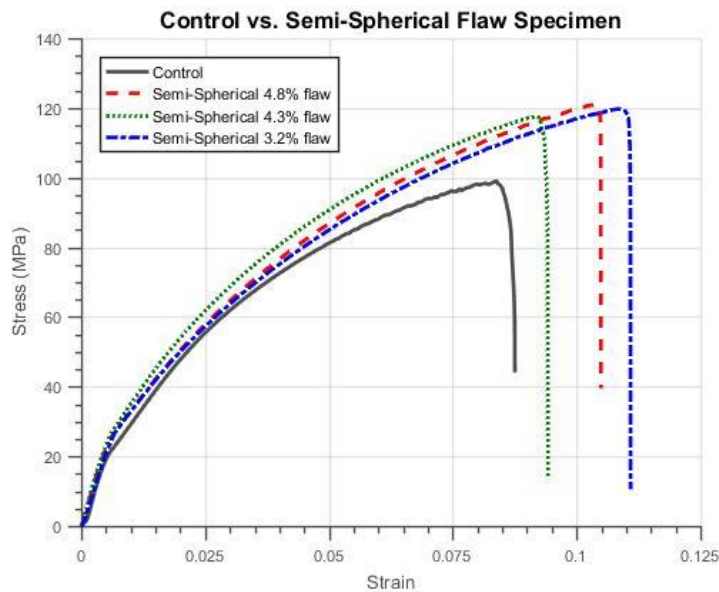


Figure 3-14: Semi-Spherically Shaped Flaw Stress-Strain Curves

The ductility was again measured and is displayed in Figure 3-15. Much like the results obtained for the spherically flawed specimens, the results for the semi-spherical specimens show a noticeable increase in ductility over the control specimen. This increase in ductility is

seen for specimens with up to 4.8% cross-sectional area removed by the surface flaw. While the results here are not as dramatic as those for the spherically shaped flaw specimens, an increase in ductility of over 50% is still evident in the specimen with 3.2% cross-sectional removed.

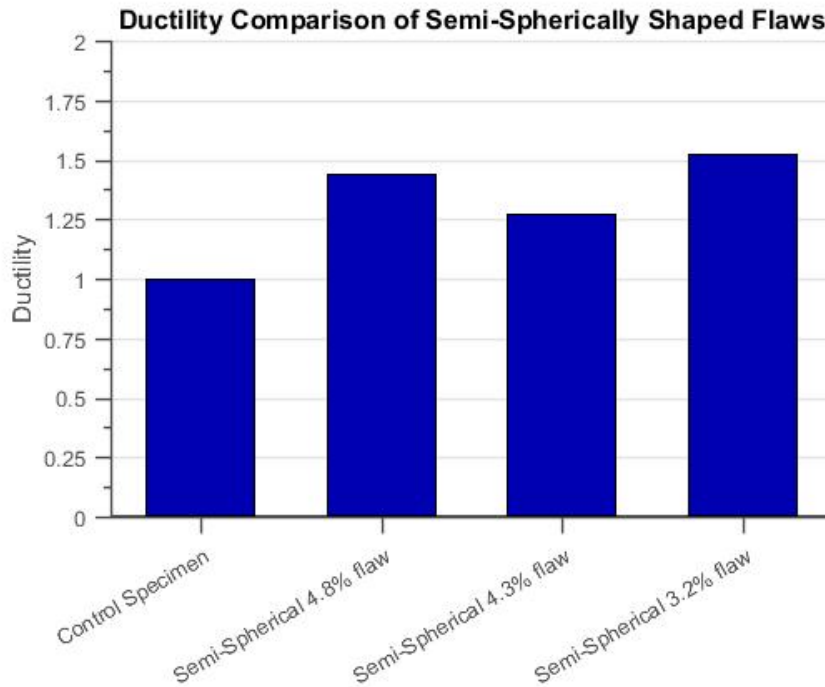


Figure 3-15: Ductility of Specimens with Semi-Spherically Shaped Flaws

An additional measurement of ductility is again calculated using the maximum and yield strains of the specimen and the results are depicted in Figure 3-16. This figure again demonstrates a general increase in ductility for specimen with semi-spherically shaped flaws. It is seen that for this shape of flaw with 3.2% of the cross-sectional area removed an increase in ductility of approximately 25% is observed. Again, while not as extreme as the results from the spherically shaped flaws, a definitive increase in ductility is observed. This result is again not

expected, but reinforces the idea that ideally shaped surface flaws can serve to increase material performance in terms of material ductility.

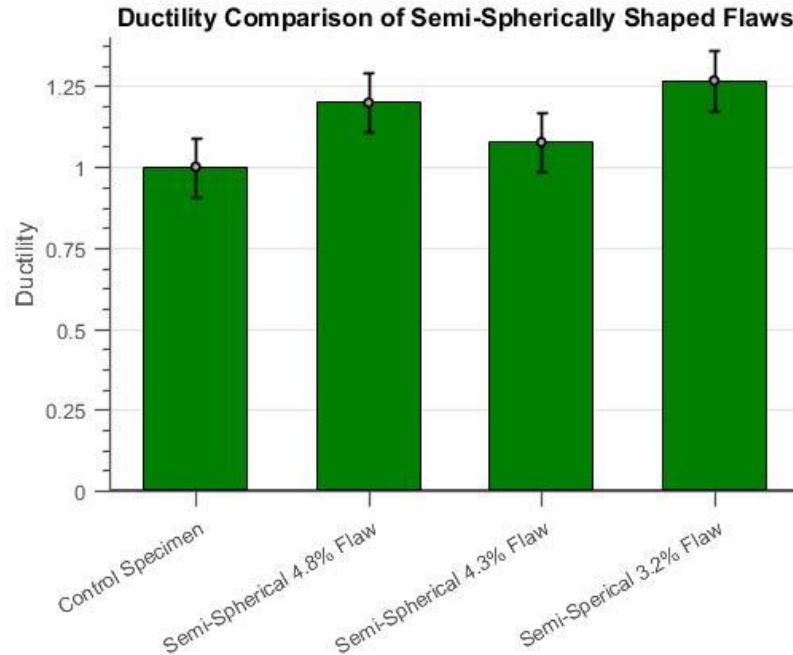


Figure 3-16: Additional Measurement of Ductility of Semi-Spherically Shaped Flaws

3.3.5 Cubically Flawed Specimen

The final set of three specimens tested were those with embedded cubically shaped surface flaws. While the “cube” designation does not accurately describe the shape of the flaws tested, the nomenclature is adopted for ease of use based on the shape of the object used to create the flaw. This cubic shape was chosen to test the effect of a flaw’s “sharpness” on the ductile fracture process. In fracture mechanics, measurements of the angle at which a crack tip terminates are often taken to be used in the prediction of crack growth throughout the fracture process. When this angle is large the crack tip is described as blunt and when it is small the crack tip is described as sharp. In a comparable way, the use of the cube shape leads

to much sharper edges in the surface flaw of the specimen than the spherical or semi-spherical shaped flaws. The results for this set of data is again normalized in similar fashion and shown alongside that of control specimen one as depicted in Figure 3-17. The results shown in Figure 3-17 display the expected decrease in maximum strain with removal of cross-sectional area of each specimen similar to the results obtained for the specimens with randomly shaped flaws.

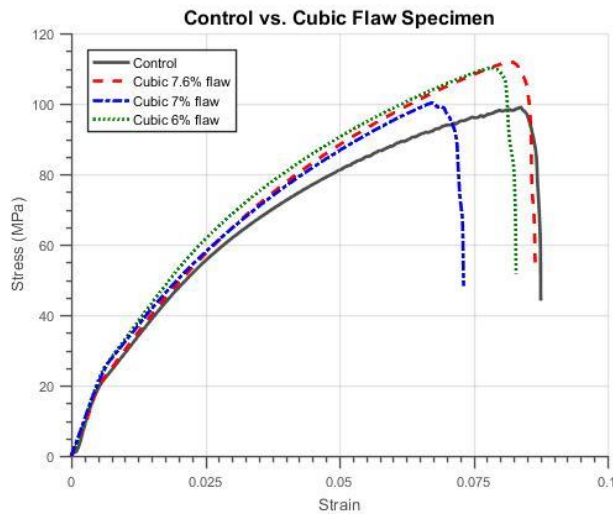


Figure 3-17: Cubically Shaped Flaw Stress-Strain Curves

To get a better overall picture for the performance of these specimens the ductility was measured and is shown in Figure 3-18. From these results, it can be noted that all of the cubically flawed specimens performed nearly the same as the control specimen, even with up to 7.6% of their cross-sectional area missing. This observation would suggest that even shapes with some inherent sharpness may be capable of increasing material performance.

Unfortunately, there are no specimens with less than 6% of their cross-sectional area removed in this data set. This lack of data makes it impossible to say whether this suggestion will hold true or not.

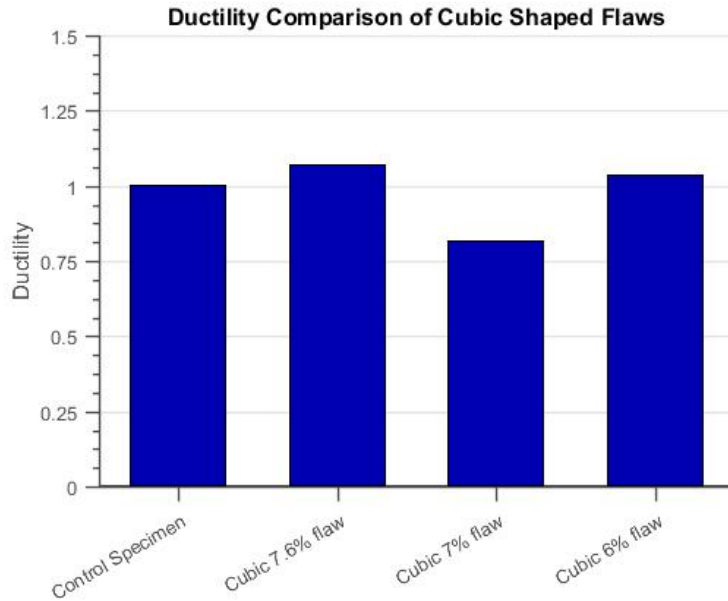


Figure 3-18: Ductility of Specimens with Cubically Shaped Flaws

An additional measurement of ductility is again calculated and the results are depicted in Figure 3-19. These results also show a general decrease in ductility for specimen with cubically shaped flaws and suggest the potential for increased ductility with smaller flaw sizes. Again, because there are not more specimens with smaller cubically shaped flaws it is impossible to tell if this suggestion would hold true or not. Although the expected results of a general decrease in ductility for specimen with cross-sectional area removed seems to hold for these cubically shaped flaws, the results are not plentiful or clear enough to make any definitive conclusions for this particular shape.

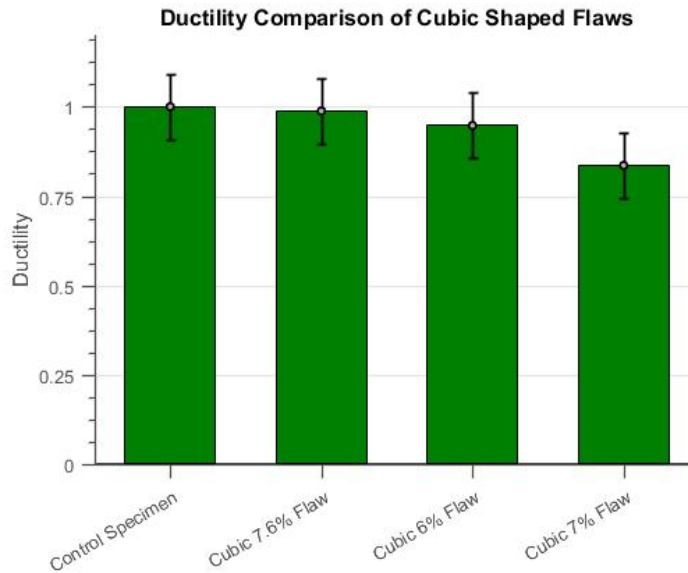


Figure 3-19: Additional Measurement of Ductility for Cubically Shaped Flaws

3.4 Fractography

After primary testing was concluded, the SEM was used to take micrographs of the fracture surfaces for each category of surface flaw. Figure 3-20 shows the fracture surface for control specimen 3 alongside that of a cast aluminum fitting that had been in useful service for more than 20 years. As can be seen in these images the fracture surface of the tested material exhibits many of the same characteristics of a cast aluminum piece that was put into service. Here the yellow arrows indicate regions of potentially brittle fracture while the black arrows indicate regions that exhibit fracture of a more ductile nature. This observation leads to the conclusion that the tested material underwent fracture in the transition region of brittle to ductile fracture.

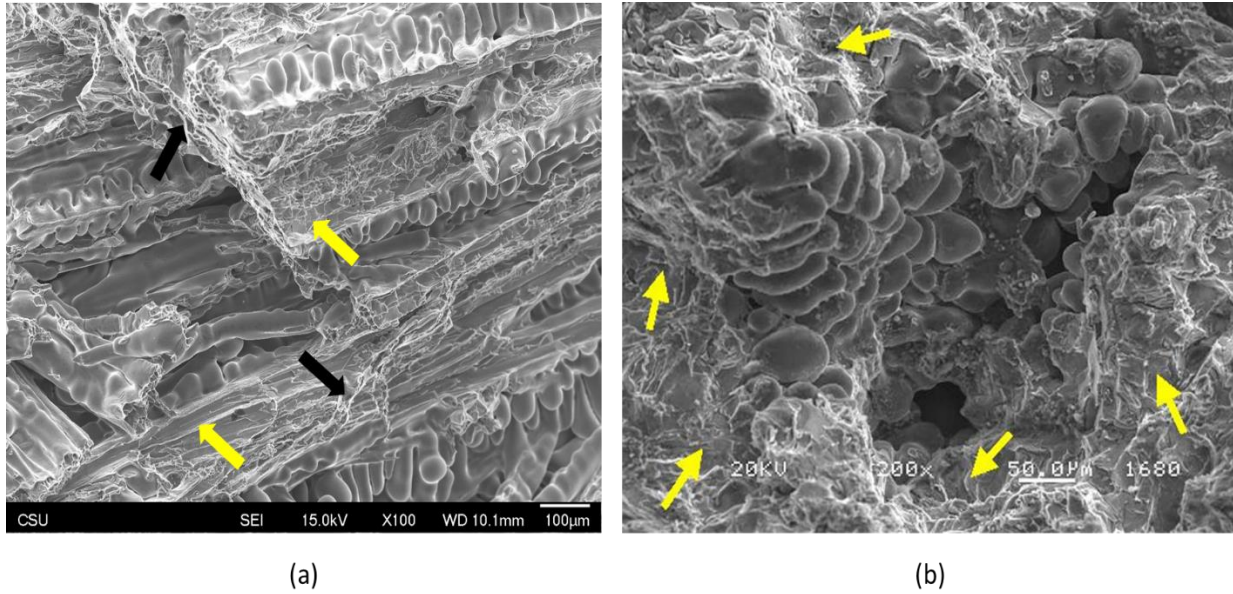
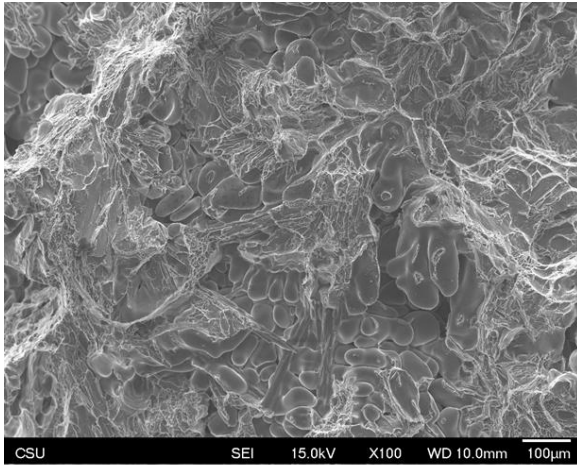
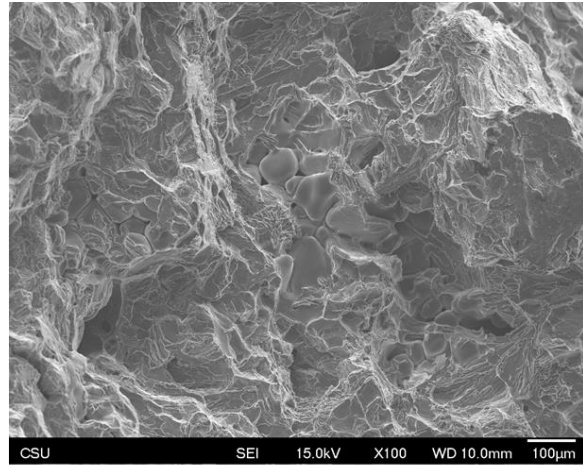


Figure 3-20: Fracture surface of (a) Control Specimen 3 and (b) Cast Aluminum Fitting

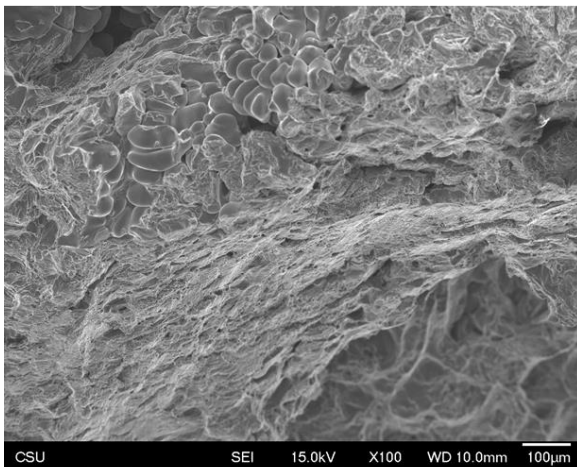
Similar results can be seen in Figure 3-21 for specimen with each distinct shape of surface flaw. Many of the same indications of brittle and ductile fracture can be seen in these images, but for the spherical and semi-spherical surface flaw specimens a much greater percentage of the fracture surface indicates ductile fracture. These images suggest that the shape of the surface flaw greatly impacts the overall ductility of the material being tested similar to the results obtained from testing.



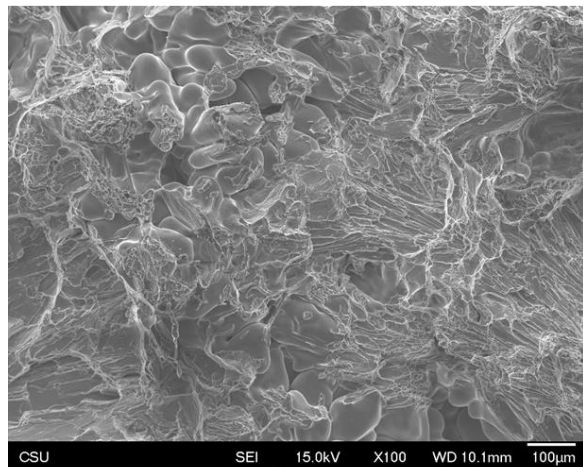
(a)



(b)



(c)



(d)

Figure 3-21: Fracture Surface of a (a) Random Surface Flaw, (b) Cubic Surface Flaw, (c) Spherical Surface Flaw and (d) Semi-Spherical Surface Flaw

3.5 General Discussion

Through examination of the results for each type of specimen, it is suggested that smooth ordered surface flaws, such as the spherical and semi-spherical flaws tested, have the ability to enhance material performance in the case of ductility. This suggestion is based on the results from each individual flaw's data sets and the micrograph images taken for each flaw shape. The suggestion that smooth ordered surface flaws can enhance material performance is

further aided when the results of several shapes are compared simultaneously. Figure 3-22 shows a select set of data for all specimens tested with 3% to 3.3% removal of cross-sectional area from the overall cross-section. It is clear to see that for specimens in this range of missing cross-sectional area, the flawless control specimen creates a clear dividing line between the maximum strain of randomly shaped surface flaws and those of an “ordered” nature.

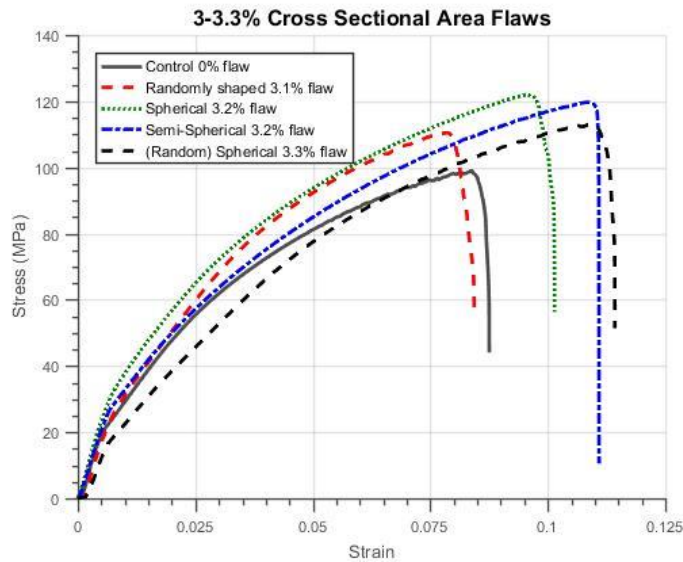


Figure 3-22: Stress-Strain Curves for Flaws Measuring 3-3.3% Cross-Sectional Area

The ductility of the specimens with flaws in the 3% to 3.3% range was also measured and is shown in Figure 3-23. This figure demonstrates the clear difference in ductility of randomly shaped surface flaws and those of an “ordered” nature. While each specimen has very nearly the same amount of cross-sectional area removed, the specimens with spherical and semi-spherical flaws demonstrate an increase of more than 35% over that of the randomly shaped flaw.

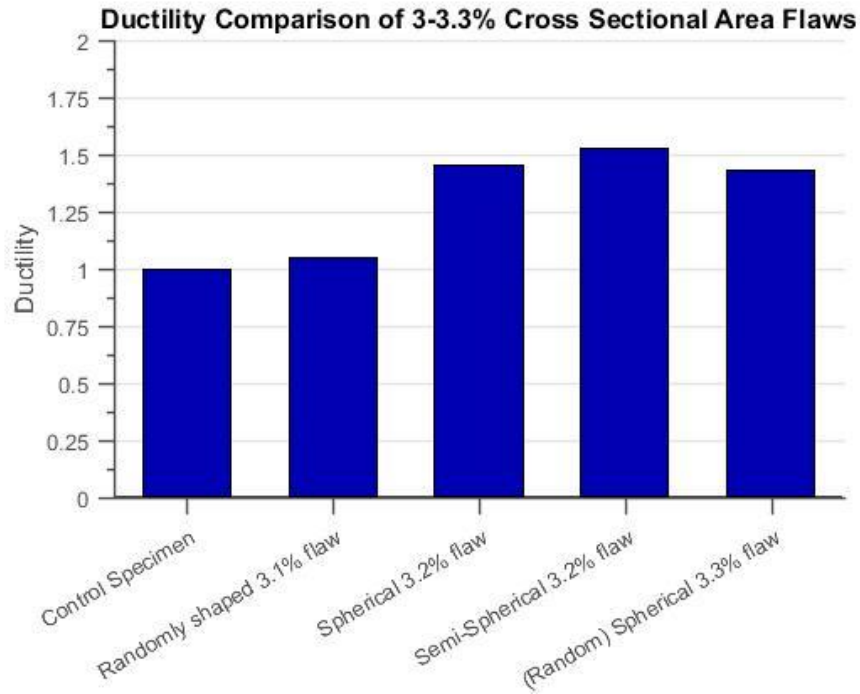


Figure 3-23: Ductility of Specimens with Flaws Measuring 3-3.3% Cross-Sectional Area

Figure 3-24 shows the same specimen being compared with the additional measurement of ductility taken from the maximum and yield strains of each specimen. The results from this additional calculation again show a clear difference in specimen with randomly shaped flaws and those with flaws of more ordered nature. It can be seen that specimen with spherical or semi-spherical flaws can demonstrate an approximate increase in ductility of 25%.

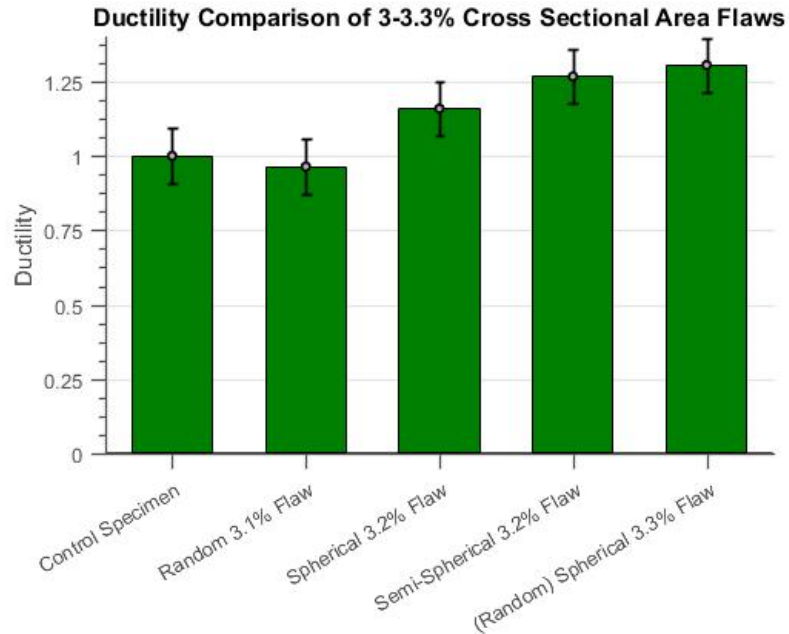


Figure 3-24: Additional Measurement of Ductility of Specimens with Flaws Measuring 3-3.3% Cross-Sectional Area

For clarity of results depicted in Figure 3-22, 3-23 and 3-24, it is necessary to explain that because of the method used in forging the randomly shaped flaw specimen, the fourth specimen created in this category turned out to be spherical in shape. This occurred because no part of the shaped aluminum flaw was included in the cross-section of this particular specimen. Therefore, the spherical glass bead was the only contribution to flaw shape. This happy coincidence further aids the argument that specific shapes can increase material performance, namely ductility, through the apparent repeatability of results.

The idea that specific shapes can increase material performance can be further explored if the surface flaws in this study are viewed in the same way as internal voids in the material. In many ductile fracture studies, a unit cell that is composed of the material matrix and a single void is used to examine fracture behavior. This unit cell can be seen in the works of Gurson

(1977), Tvergaard and Needleman (1984), Gao et al. (2005) and many others. This single cell of material is given some representative volume within an entire test volume and a representative void volume that takes up some of that space. This cell is then analyzed for fracture behavior and the results are extrapolated and imposed on similar cells that are used to fill the remaining material volume in question. While this method is most commonly used in the analysis of voids on a micro-scale, there is no apparent reason, besides computational limitations, that it cannot be used to analyze voids in a much larger scale with an equally fine material matrix. In this way, the single flaws embedded in the specimens for the current study can be viewed as the single voids in a unit cell of representative material volume that would take up much of the reduced section of each specimen.

The second consideration that needs to be addressed in order for the surface flaws to be considered as similar to internal voids in the material is the fact that they are surface flaws. This matter can be handled by the idea of symmetry. In many cases of finite element modeling, computational limitations are addressed through the use of symmetry. If the geometry of the problem in question, a void in this case, is symmetric about a single plane and the boundary conditions are the same for each half of the model, then only one half of the model needs to be solved in order to solve the entire problem. For the specimen in this study, the nature of testing assumes that equal force is exerted on the entire cross-sectional area of the specimen in uniaxial tension. If this specimen was to be made twice as thick or made much thinner and tested in the same manner the same assumption would apply. If a specimen in this study is then viewed as only one half of a total specimen, the requirement of boundary conditions and symmetry apply and only one half of the specimen needs to be analyzed.

With these two conditions met, some basis for surface flaw and internal void similarity is established. The research conducted by Tvergaard and Hutchinson (2002) then becomes a starting point that may help to explain the increase in material ductility observed in the current research. Their research suggested two mechanisms for ductile crack growth. In particular, it was seen that for materials with large initial void volume, which is the case for the current study, crack propagation proceeded by a multiple void interaction mechanism. While this can mean faster crack growth, it also allows for secondary cracks to open away from the initial crack and sometimes even in planes near, but not on, the fracture plane. This may in turn promote slower crack propagation. Goa et al. (2005) continued on this work and noticed that oblate voids grew faster than spherical voids when other parameters were constant. This observation would lead to slower crack propagation for spherical voids and delay the onset of failure. While either of these cases may be used to explain the difference in ductile behavior between different flaw shapes, neither of them suggest that any specimen should exhibit more ductility than a control specimen with no initial flaws.

Assuming the established link between surface flaw and internal void holds, the results from this experiment suggest that ideally shaped voids used in most ductile fracture studies may not behave in the exact manner assumed. If voids were ideally shaped in real materials, like the aluminum tested in this study, those materials may exhibit ductility that is noticeably larger than their randomly shaped void counterparts. This means that any model utilizing these ideally shaped voids would almost certainly demonstrate higher ductility, or strain at fracture, than physical testing would indicate. While the over prediction of fracture strain does appear to occur, it seems nearly as likely that an under prediction will occur. This can be seen in

numerous studies including those conducted by Bao (2003), Bai and Wierzbicki (2010) and Wen and Mahmoud (2015a). The apparent inconsistency in prediction values lends strength to the argument that idealized void shapes may not behave as predicted in the past. This conclusion suggests that any existing ductile fracture models that utilize these idealized void shapes would inherently give incorrect fracture prediction values because actual void geometry plays a major role in the ductile fracture process as the results from this study suggest.

3.6 Secondary Cracking

An additional observation made in the current study is the formation of secondary cracks in the specimens that exhibited higher ductility than the control specimen. These secondary cracks were noticed opening at a considerable distance away from the initial surface flaw for those specimens and exhibited no apparent interaction with the fracture plane. Every secondary fracture is also unique in both size and distance from the fracture plane with one instance measured 14mm from that plane. Some examples of this fracture pattern are depicted in Figure 3-25 with red arrows highlighting some of the secondary cracks observed.

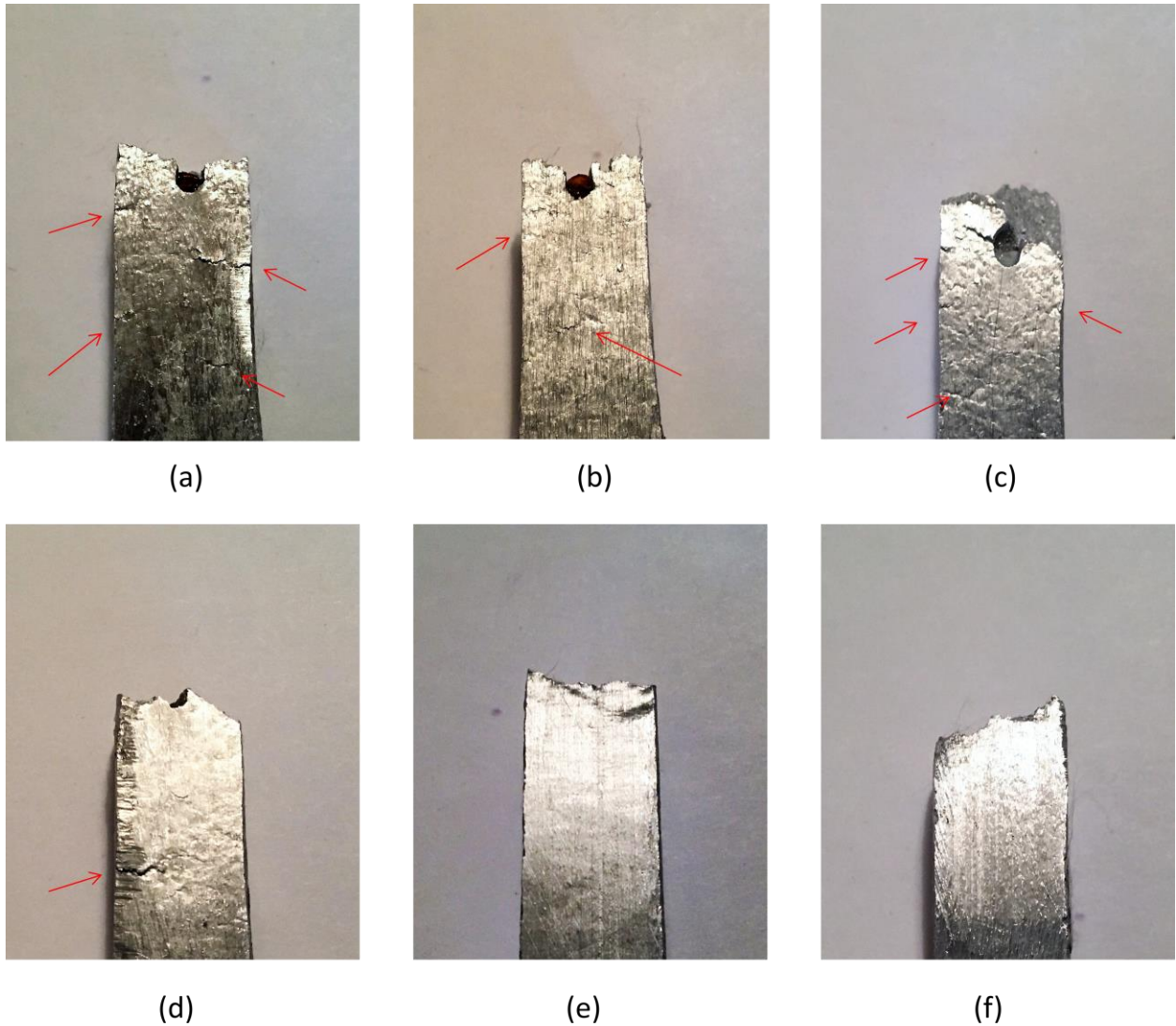


Figure 3-25: Secondary Cracking as Observed for (a) Semi-Spherical Specimen 1 (b) Semi-Spherical Specimen 2 (c) Spherical Specimen 2 (d) (Random) Spherical Specimen 4 and Lack of Secondary Cracking for (e) Control Specimen 3 (f) Random Specimen 7

The lack of secondary crack formation in all specimens with ductility measured less than that of the control specimen, including the control specimens themselves, is also noteworthy. This observation is a strong indicator that the shape of the surface flaw is the vital variable that leads to improved ductility in the material tested. As can be seen in Figure 3-22 and 3-23, randomly shaped surface flaws of similar size to the idealized spherical surface flaws do not

behave in a similar fashion. Since these randomly flawed specimens do not exhibit the same secondary cracking, it is reasonable to conclude that the secondary cracks, presumably caused by flaw shape, are the reason ductility is increased in the spherically and semi-spherically flawed specimens.

The secondary cracking observed for the “ideally” shaped surface flaw specimens is thought to release stress buildup in the specimen by redirecting it elsewhere. This appears to be the case since every specimen that showed signs of secondary crack formation failed at the initially embedded surface flaw and not a secondary crack. While this secondary cracking is almost certainly due to flaw shape, it may be possible to link the secondary cracks to the multiple void interaction mechanism discussed previously. If the surface flaws are assumed to be one half of the symmetric representation of a single void in a rather large unit cell material matrix, then the multiple void interaction mechanism would allow for secondary crack formation as void interaction away from the fracture plane. The seemingly random location and size of the secondary cracks noted in the flawed specimen of “ideal” shape helps to support this theory.

3.7 Ductility Profile

The aluminum tested in this study demonstrates a unique ductility “profile”, as seen through the stress-strain curves obtained, that is consistent with expectations set by similar profiles seen in testing of many other grades of aluminum. This similarity is seen specifically in the way that aluminum tends to take loading up to some maximum stress then quickly fails with minimal additional strain. The similarity discussed can be seen by comparing the results

from the control specimen of this study to similar results for other aluminum as depicted in Figure 3-26.

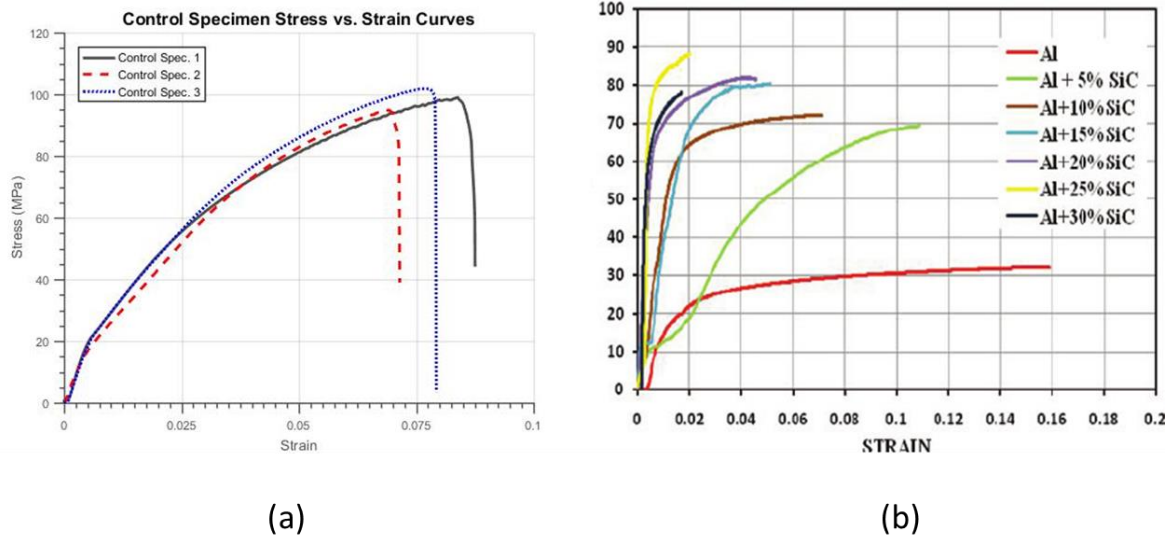


Figure 3-26: Stress Strain Curves for (a) Control Specimens and (b) Varying Aluminum Alloys (Singh et al 2015)

The results collected from testing in this study suggest that it may be possible to increase material performance in terms of ductility, maximum attainable stress and maximum attainable strain for ductile aluminum alloys that demonstrate similar ductility profiles by inserting specifically shaped flaws. This suggestion might also be made for any ductile material that demonstrates a similar ductility profile and is used in uniaxial tension and monotonic loading conditions similar to testing conditions seen in this study.

3.8 Conclusion

This study explored, through physical testing of a single batch of grade 6061 aluminum, the effects of four uniquely shaped surface flaws on the ductile fracture process. Based on the results obtained the following conclusions are made.

Through the use of stress-strain curves obtained for each specimen and micrograph images from a SEM, a noticeable effect on ductility is observed. For specimens with randomly shaped surface flaws the overall ductility of the material decreases as increased portions of the specimen's cross-sectional area are removed. This result confirms classical expectations and the trend seen in the work conducted by Spannaus (2016). This result is not consistent for specimens with surface flaws resembling the idealized shapes often used to describe void shape in ductile fracture modeling. For these specimens, the results show a trend of increased performance over the control specimen tested with up to 3.2% cross-sectional area removed by the flaw. This is seen both in terms of overall ductility and maximum attainable stress and strain values.

Through the previous conclusion, a strong dependence of flaw shape on the ductile fracture process can be noted. Further evidence to support this dependence is seen through secondary crack formation in spherically and semi-spherically shaped surface flaw specimens. These two shapes promote the generation of secondary cracks that appear to allow for stress redistribution within the specimen delaying the fracture process. An absence of any secondary crack formation in other flaw shapes tested is also noted.

It is suggested that any ductile material with a similar ductility profile, as seen through the stress-strain curve, and testing conditions to those seen in this study may have its overall performance enhanced through the inclusion of idealized surface flaws. This suggestion cannot yet be made for any material whose ductility profile does not match that of the aluminum tested since many materials do not fail very shortly after reaching some maximum stress value.

Some similarity can be seen between internal voids and surface flaws. Through the consideration of geometry, it may be possible to attribute the fracture process of a spherically shaped surface flaw of sufficient volume to the multiple void interaction mechanism explored by Tvergaard and Hutchinson (2002). The use of the unit cube and symmetrical modeling often employed in micromechanical void research also lend themselves nicely to this point since the scale in which they are applied is not specifically limited. With this and the importance of void shape on the ductile fracture process in mind it can be seen that existing ductile fracture models that employ the use of idealized void shapes could be much improved by the modeling of more complex shapes.

CHAPTER 4

CONCLUSION & FUTURE WORK

The ductile fracture of structural materials is of great concern to the engineering community. The ductile failure of materials is evident in many real-world scenarios and many models have been suggested in an attempt to predict this failure process. While an abundance of research has been conducted on this subject, limited experimental research has been conducted on the effects of actual void shape and specifically shaped, three-dimensional surface flaws on the ductile fracture process.

In an attempt to explore these areas of research, a simple uniaxial tension test was proposed to study the effect of surface flaw shape on the ductile fracture process. A simple coal fire forge was constructed and a single batch of recycled structural grade 6060 aluminum was utilized to create dogbone test specimens according to the ASTM standards. Four unique surface flaw shapes were proposed to mimic idealized void shapes observed in the literature and random void shapes observed in real materials. The material used for the shapes to be embedded in the specimen was also proposed to be made of glass. This would ensure that the shape would hold in the forging process since the melting point of glass is higher than that of the aluminum used and that minimal material interaction would be observed. These shapes were also given varying volumes within the test specimens in an effort to test volume as an additional variable.

Each specimen forged was tested in uniaxial tension and data was collected in the form of stress-strain curves. These curves were then used to analyze material performance with

respect to overall ductility and maximum attained stress. Comparison of these curves was then conducted between each unique flaw shape and the group of control specimens and used to analyze the effect of each shape.

Three control specimens were tested and the resulting stress-strain curves were analyzed for use as a baseline for comparison. These specimens exhibited some amount variability which was to be expected due to material variability introduced through the forging and casting process. The specimen that performed best was used as a comparative baseline for the remaining tests.

A total of eight specimens with randomly shaped surface flaws were tested and their resulting data was analyzed. The resulting stress-strain curves were tested against the chosen control specimen. The results suggest that overall ductility of the material decreases with increasing amounts of cross-sectional area removed by the flaw. This conclusion fits in well with previously recorded experimental data and, like the control specimen, displays good agreement with expectation.

Data was also collected from three spherically shaped surface flaw specimens and three semi-spherically shaped surface flaw specimens. While the resulting stress-strain curves for these specimens indicate their own unique effects on ductile fracture, they both exhibit a noticeable increase in overall ductility when compared to the control specimen. This is perhaps the most interesting result to be recorded as no suggestions of this seemed to be made in the literature. These results confirm the extreme importance of flaw shape on the ductile fracture process and suggest it may be possible to increase overall material performance through

strategically placed surface flaws in materials that have similar ductility profiles as the aluminum tested. It was noted during testing that, because of the way the randomly shaped flaws were created, one of the specimens containing randomly shaped flaws was actually spherical. The results obtained for this specimen agreed with those for the spherical and semi-spherical flaws. This apparent repeatability of results stands as some confirmation of results and conclusions drawn from the spherically and semi-spherically flawed specimens.

Three specimens containing cubically shaped flaws were also tested. The results from these tests exhibited very similar performance to those of the control specimen even with significant cross-sectional area removal. This suggests that it may be possible for the surface flaws to display superior performance over control specimens much like the spherical surface flaws did. The results from these specimens however are largely inconclusive due to a lack of sufficient data.

Also of note was the observation of secondary cracks opening away from the initial flaw and fracture plane. These secondary cracks had no apparent interaction with the fracture plane and in some cases, were seen opening at great distances from the initial flaw. The secondary cracks were also noted to appear in random locations and grew to random size before the specimen eventually failed at the initial surface flaw. It is theorized that the secondary cracks observed are responsible for the increased ductility observed in some flaw shapes since cracking was only observed for those specimen that exhibited increased ductility.

It is theorized that surface flaws behave in similar ways to internal material voids. The secondary cracking observed could be an indication of the multiple void interaction mechanism

used to describe void growth and coalescence in the literature. With this noted it would not be a large leap to arrive at this conclusion.

The results from this research suggest many ideas, but the researcher is aware that limited sample size and data collected make it difficult to conclusively prove any of the results found. Future work and testing is required to confirm these results and alternate materials and methods for specimen fabrication are suggested. This study focused on the effect of surface flaws on the ductile fracture process, specifically as it pertained to overall material ductility. There are many other aspects of the ductile fracture process that may be considered. It would also be worth exploring the effect of similar shapes embedded as internal flaws for future work as it is thought that similar results may be obtained.

WORKS CITED

- Aravas, N., McMeeking, R.M., 1985a. Finite element analysis of void growth near a blunting crack tip. *J. Mech. Phys. Solids* 33, 25–49.
- Aravas, N., McMeeking, R.M., 1985b. Microvoid growth and failure in the ligament between a hole and blunt crack tip. Finite element analysis of void growth near a blunting crack tip. *Int. J. Fract.* 29, 21–38.
- Argon, A. S., Im, J., 1975. Separation of second phase particles in spheroidized 1045 steel, Cu-0.6pct Cr 704 Alloy, and maraging steel in plastic straining. *Metallurgical Transactions* 6A, 839-851. 705
- Arun Roy, Y., Narasimhan, R., 1999. A finite element investigation of the effect of crack tip constraint on hole growth under mode I and mixed mode loading. *Int. J. Solids Struct.* 36, 1427–1447.
- Bai, Y., 2008. Effect of loading history in necking and fracture (Doctoral dissertation, Massachusetts Institute of Technology). 709
- Bai, Y., Teng, X., Wierzbicki, T., 2009. On the application of stress triaxiality formula for plane strain fracture testing. *Journal of Engineering Materials and Technology*, 131(2), 021002. 711
- Bai, Y., Wierzbicki, T., 2008. A new model of metal plasticity and fracture with pressure and Lode dependence. *International Journal of Plasticity*, 24(6), 1071-1096. 713
- Bai, Y., Wierzbicki, T., 2010. Application of extended Mohr–Coulomb criterion to ductile fracture. *International Journal of Fracture*, 161(1), 1-20. 715

- Bao, Y., 2003. Prediction of ductile track formation in uncracked bodies (Doctoral dissertation, 716 Massachusetts Institute of Technology). 717
- Bao, Y., Treitler, R., 2004. Ductile crack formation on notched Al2024-T351 bars under compression–718 tension loading. *Materials Science and Engineering: A*, 384(1), 385-394. 719
- Bao, Y., Wierzbicki, T., 2004. On fracture locus in the equivalent strain and stress triaxiality space. *International Journal of Mechanical Sciences*, 46(1), 81-98. 721
- Bao, Y., Wierzbicki, T., 2005. On the cut-off value of negative triaxiality for fracture. *Engineering fracture mechanics*, 72(7), 1049-1069. 723
- Barsoum, I., Faleskog, J., 2007. Rupture mechanisms in combined tension and shear—experiments. *International Journal of Solids and Structures*, 44(6), 1768-1786. 725
- Benzerga, A., Leblond, J. B., 2010. Ductile fracture by void growth to coalescence. *Advances in Applied Mechanics*, 44, 169-305. 729
- Bermin, F. M., 1981. Cavity formation from inclusions in ductile fracture. *Metallurgical Transactions* 12 A, 730 723-731. 731
- Brown, L.M., Embury, J.D., 1973. In: *Proceedings of the 3rd International Conference on Strength of Metals and Alloys*. Institute of Metals, London, p. 164.
- Brozzo, P., Deluca, B., Rendina, R., 1972. A new method for the prediction of formability limits in metal 732 sheets. In *Proc. 7th biennial Conf. IDDR*. 733
- Chu, C., Needleman, A., 1980. Void nucleation effects in biaxially stretched sheets. *Journal of Engineering Materials and Technology* 102, 249-256. 735

- Clift, S. E., Hartley, P., Sturgess, C. E. N., Rowe, G. W., 1990. Fracture prediction in plastic deformation processes. *International Journal of Mechanical Sciences*, 32(1), 1-17. 737
- Cockcroft, M. G., Latham, D. J., 1968. Ductility and the workability of metals. *J Inst Metals*, 96(1), 33-39. 738
- Faleskog, J., Gao, X., Shih, C.F., 1998. Cell model for nonlinear fracture analysis—I. Micromechanics calibration. *Int. J. Fract.* 89, 355–373.
- Gao, X., Faleskog, J., Shih, C.F., 1998a. Cell model for nonlinear fracture analysis—II. Fracture-process calibration and verification. *Int. J. Fract.* 89, 375–398.
- Gao, X., Faleskog, J., Shih, C.F., Dodds, R.H., 1998b. Ductile tearing in part-through cracks: experiments and cell-model predictions. *Eng. Fract. Mech.* 59, 761–777.
- Gao, X., Zhang, T., Hayden, M., Roe, C., 2009. Effects of the stress state on plasticity and ductile failure of an aluminum 5083 alloy. *International Journal of Plasticity*, 25(12), 2366-2382. 743
- Gao, X., Wang, T., Kim, J. 2005. On ductile fracture initiation toughness: Effects of void volume fraction, void shape and void distribution. *Int. J. of solids and structures* 42 (18-19): 5097-5117.
- Gologanu, M., Leblond, J. B., Devaux, J., 1993. Approximate models for ductile metals containing spherical voids—case of axisymmetric prolate ellipsoidal cavities. *Journal of the Mechanics and Physics of Solids*, 41(11), 1723-1754. 746

- Gologanu, M., Devaux, J., Leblond, J. B., 1994. Approximate models for ductile metals containing 747 nonspherical voids—case of axisymmetric oblate ellipsoidal cavities. *Journal of Engineering Materials and Technology*, 116(3), 290-297. 749
- Gologanu, M., Leblond, J. B., Perrin, G., Devaux, J., 1998. Recent extensions of Gurson's model for 750 porous ductile metals. In *Problèmes non linéaires appliqués. Ecoles CEA-EDF-INRIA*, 134-203. 751
- Gu, I., 2000. Finite element analyses of the deformation around holes near crack tip and their implications to the J-resistance curve. *Fatig. Fract. Eng. Mater. Struct.* 23, 943–952.
- Gurson, A.L., 1977. Continuum of ductile rupture by void nucleation and growth: Part I—Yield criteria and flow rules for porous ductile media. *J. Eng. Mater. Tech.* 99, 2–55.
- Hom, C.L., McMeeking, R.M., 1989. Void growth in elastic–plastic materials. *J. Appl. Mech.* 56, 309–317.
- Johnson, G. R., Cook, W. H., 1985. Fracture characteristics of three metals subjected to various strains, 755 strain rates, temperatures and pressures. *Engineering fracture mechanics*, 21(1), 31-48. 756
- Khan, A. S., Liu, H., 2012. A new approach for ductile fracture prediction on Al 2024-T351 alloy. 761 *International Journal of Plasticity*, 35, 1-12. 762
- Kim, J., Gao, X., Srivatsan, T.S., 2003. Modeling of crack growth in ductile solids: a three-dimensional analysis. *Int. J. Solids Struct.* 40, 7357–7374.
- Kim, J., Gao, X., Srivatsan, T.S., 2004. Modeling of void growth in ductile solids: effects of stress triaxiality and initial porosity. *Eng. Fract. Mech.* 71, 379–400.

- Kiran, R., Khandelwal, K., 2014. A triaxiality and Lode parameter dependent ductile fracture criterion. *Engineering Fracture Mechanics*, 128, 121-138. 764
- Koplik, J., Needleman, A., 1988. Void growth and coalescence in porous plastic solids. *Int. J. Solids Struct.* 24, 835–853.
- Ko, Y. K., Lee, J. S., Huh, H., Kim, H. K., Park, S. H., 2007. Prediction of fracture in hub-hole expanding process using a new ductile fracture criterion. *Journal of materials processing technology*, 187, 358-766 362. 767
- Lee, B. J., Mear, M. E., 1999. Stress concentration induced by an elastic spheroidal particle in a plastically deforming solid. *Journal of the mechanics and Physics of Solids* 47, 1301-1336. 771
- Le Roy, G., Embury, J.D., Edward, G., Ashby, M.F., 1981. A model of ductile fracture based on the nucleation and growth of voids. *Acta Metall.* 29, 1509–1522.
- Liu, T., Lin, B., Yang, W., Zou, Q., Kong, J. and Yan, F. 2016 Cracking Process and Stress Field Evolution in Specimen Containing Combined Flaw Under Uniaxial Compression. *Rock Mechanics and Rock Engineering* 49 (8): 3095-3113.
- McClintock, F. A., 1968. A criterion for ductile fracture by the growth of holes. *Journal of applied mechanics*, 35(2), 363-371. 782
- Oh, S. I., Chen, C. C., Kobayashi, S., 1979. Ductile fracture in axisymmetric extrusion and drawing—part 2: workability in extrusion and drawing. *Journal of Engineering for Industry*, 101(1), 36-44. 786
- Oyane, M., Sato, T., Okimoto, K., Shima, S., 1980. Criteria for ductile fracture and their applications. *Journal of Mechanical Working Technology*, 4(1), 65-81. 788

- Rice, J.R., Johnson, M.A., 1969. The role of large crack tip geometry changes in plane strain fracture. In: Kannine, M.F., Adler, W.F., Rosenfield, A.R., Jaffee, R.I. (Eds.), *Inelastic Behavior of Solids*. McGraw-Hill, New York, p. 641.
- Rice, J. R., Tracey, D. M., 1969. On the enlargement of voids in triaxial stress fields. *Journal of the 789 mechanics and Physics of Solids* 17, 201-217. 790
- Singh, V. K., et al. "Enhancement of Wettability of Aluminum Based Silicon Carbide Reinforced Particulate Metal Matrix Composite." *High Temperature Materials and Processes* 34.2 (2015): 163-170.
- Spannaus, M., 2016. Structural safety check for products made of cast steel. In: Submitted Phd. thesis, Karlsruhe Institute of Technology, Department of Civil Engineering, Geo and Environmental Sciences. Karlsruhe.
- Thomason, P. F., 1968. A theory for ductile fracture by internal necking of cavities. *J. Inst. Metals* 96, 799 360-365. 800
- Thomson, C.I.A., Worswick, M.J., Pilkey, A.K., Lloyd, D.J., 2003. Void coalescence within periodic clusters of particles. *J. Mech. Phys. Solids* 51, 127–146.
- Tvergaard, V., 1982. On localization in ductile materials containing spherical voids. *Int. J. Fract.* 18, 237–252.
- Tvergaard, V., Hutchinson, J.W., 2002. Two mechanisms of ductile fracture: void by void growth versus multiple void interaction. *Int. J. Solids Struct.* 39, 3581–3597.
- Tvergaard, V., Needleman, A., 1984. Analysis of the cup-cone fracture in a round tensile bar. *Acta Metallurgica*, 32(1), 157-169. 802

- Wen, H., and Mahmoud, H. 2015a. New Model for Ductile Fracture of Metal Alloys. I: Monotonic Loading. *Journal of engineering mechanics* 142 (2): 04015088.
- Wen, H., and Mahmoud, H. 2015b New Model for Ductile Fracture of Metal Alloys. II: Reverse Loading. *Journal of engineering mechanics* 142 (2): 04015088.
- Wierzbicki, T., Bao, Y., Lee, Y. W., Bai, Y., 2005a. Calibration and evaluation of seven fracture models. *807 International Journal of Mechanical Sciences*, 47(4), 719-743. 808
- Wierzbicki, T., Bao, Y., Bai, Y., 2005b. A new experimental technique for constructing a fracture envelope 809 of metals under multi-axial loading. In *Proceedings of the 2005 SEM annual conference and 810 exposition on experimental and applied mechanics* (pp. 1295-1303). 811
- Wierzbicki, T. and Xue, L.,2005. On the Effect of the Third Invariant of the Stress Deviator on Ductile 812 Fracture, Technical Report, Impact and Crashworthiness Lab, MIT. 813
- Wilkins, M. L., Streit, R. D., Reaugh, J. E., 1980. Cumulative-strain-damage model of ductile fracture: 814 simulation and prediction of engineering fracture tests (No. UCRL-53058). Lawrence Livermore 815 National Lab., CA (USA); Science Applications, Inc., San Leandro, CA (USA). 816
- Xia, L., Shih, C.F., Hutchinson, J.W., 1995. Computational approach to ductile crack growth under large scale yielding conditions. *J. Mech. Phys. Solids* 43, 389–413.
- Xue, L., 2008. Constitutive modeling of void shear effect in ductile fracture of porous materials. 817 *Engineering Fracture Mechanics* 75,3343-66. 818
- Xue, L., Wierzbicki, T., 2008. Ductile fracture initiation and propagation modeling using damage plasticity 819 theory. *Engineering Fracture Mechanics*, 75(11), 3276-3293. 820

Xue, L., Wierzbicki, T., 2009. Ductile fracture characterization of aluminum alloy 2024-T351 using 821 damage plasticity theory. *International Journal of Applied Mechanics*, 1(02), 267-304. 822

Yan, C., Mai, U.W., 1998. Effect of constraint on void growth near a blunt crack tip. *Int. J. Fract.* 92, 287–304.

Zhang, K.S., Bai, J.B., Francois, D., 2001. Numerical analysis of the influence of the Lode parameter on the void growth. *Int. J. Solids Struct.* 38, 5847–5856.